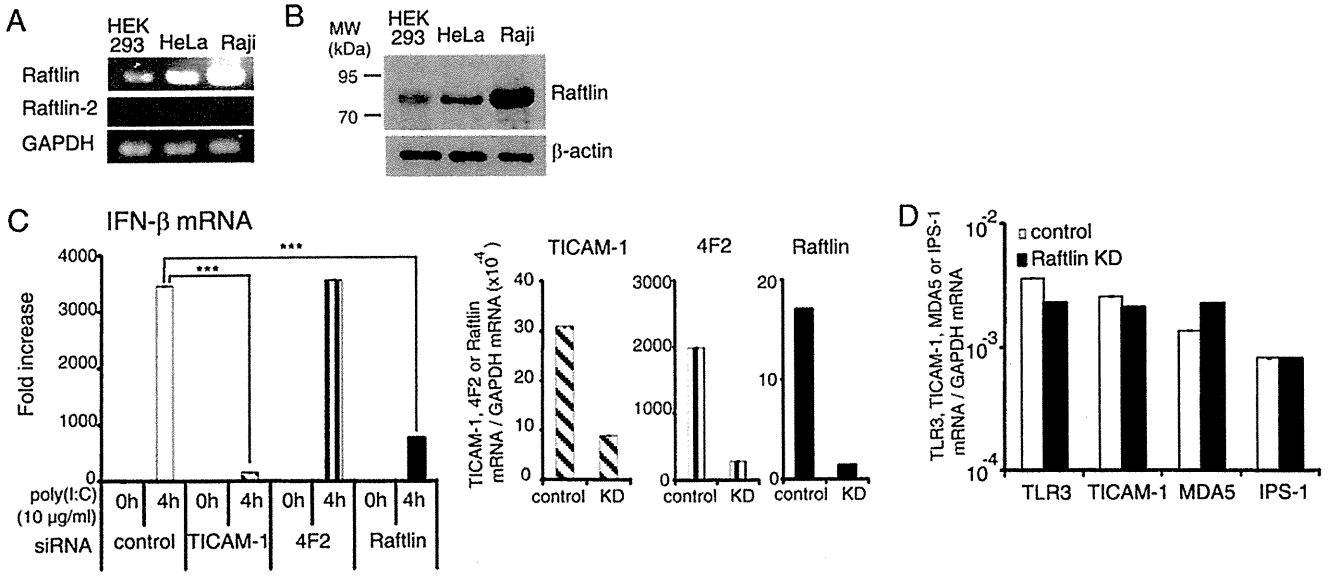

FIGURE 2. **Raftlin is essential for poly(I:C)-induced IFN-β production in HeLa cells.** *A*, expression of Raftlin and Raftlin-2 mRNAs in human cell lines. *B*, protein expression level of Raftlin in human cell lines. Cell lysates (3 μg) were separated on 10% SDS-PAGE, followed by immunoblotting with anti-Raftlin pAb or anti-β-actin mAb. *C*, poly(I:C)-induced IFN-β mRNA expression in HeLa cells. HeLa cells were transfected with the indicated siRNAs (20 pmol) using Lipofectamine 2000. Forty-eight hours after transfection, cells were washed and stimulated with 10 μg/ml of poly(I:C) for 4 h (*left-hand panel*). Total RNA was extracted and qPCR was performed using primers for the respective genes (*C* and *D*). Expression of each gene was normalized to GAPDH mRNA expression. Data are shown as the mean ± S.D., although the values are too small to represent. Representative data from three independent experiments are shown. ***, $p < 0.001$.

mixed with new poly(U)-Sepharose and rotated for 1 h at 4 °C. After centrifugation, supernatants were mixed with new poly(I:C)-Sepharose. The poly(U)- and poly(I:C)-Sepharose were washed three times with 5 volumes of washing buffer and binding molecules were eluted with elution buffer. The eluates were concentrated using YM-50 Microcon (Millipore).

Mass Spectrometry—The poly(U)- or poly(I:C)-binding molecules were separated on a 10% SDS-PAGE gel under reducing conditions, and the region of the gels containing proteins from about 250,000 to 20,000 was cut at about 1–2-mm intervals as described previously (30). After in-gel digestion with modified trypsin, the resulting peptides were analyzed by LC/MS/MS. The ion spectrum data generated by LC/MS/MS were screened against the international protein index human data base (version 3.29) with Mascot (Matrix Science, London, UK) to identify high-scoring proteins.

RNA Interference and Luciferase Reporter Assay—siRNA duplexes (LYRIC, catalog number s40866; 4F2, catalog number s12944; Raftlin, catalog numbers s23219, s23217, and s23218; negative control, catalog number AM4635) were obtained from Ambion-Applied Biosystems. siRNA for TICAM-1 was purchased from Xeragon Inc. (Birmingham, AL) (18). HEK293 cells cultured in 24-well plates were transfected with 20 pmol of each siRNA together with the expression vector for human TLR3 or TLR2 (200 ng), IFN-β promoter or ELAM reporter plasmid (60 ng), and an internal control vector (1.5 ng) using Lipofectamine 2000. Forty-eight hours after transfection, cells were washed once and then stimulated with 10 μg/ml of poly(I:C) or MALP-2 (200 nM) for 6 h. Cells were lysed and dual luciferase activities were measured according to the manufacturer's instructions (Promega). The *Firefly* luciferase activity was normalized to the *Renilla* activity and expressed as the fold-induction relative to the activity of unstimulated vector-transfected cells. In the case of HeLa cells, cells in 24-well plates were transfected with 20 pmol of each siRNA using Lipofectamine 2000. Knockdown of Raftlin in human MoDCs was preformed by electroporation as described previously (31). Briefly, MoDCs (1.4×10^6/80 μl) were transfected with control siRNA or siRNA for Raftlin (500 pmol) using a Gene-Pulser (Bio-Rad) and then cultured for 36 h in the presence of 500 milliunits/ml of granulocyte-macrophage colony-stimulating factor. The viability of the cells transfected with control and Raftlin siRNAs was 84 and 87%, respectively. Knockdown of mouse Raftlin-2 in Raftlin$^{-/-}$ BMDCs was performed with shRNA lentiviral particles (Santa Cruz) according to the manufacturer's instructions. Briefly, Raftlin$^{-/-}$ BMDCs in 24-well plates were infected with control shRNA lentiviral particles or mouse Raftlin-2 shRNA lentiviral particles at a multiplicity of infection of 2 and incubated in complete medium containing Polybrene (5 μg/ml). Twenty-four hours after infection, medium was replaced with complete medium and cells were further incubated for 24 h. The viability of the cells infected with control lentivirus and mouse Raftlin-2 shRNA-expressing lentivirus was 82 and 76%, respectively.

Quantitative PCR (qPCR)—Total RNA was extracted with the RNeasy mini kit (Qiagen, Valencia, CA) and 0.5 μg of RNA was reverse-transcribed using the high capacity cDNA Reverse Transcripition kit (Applied Biosystems) with random primers according to the manufacturer's instructions. Quantitative PCR was performed with the indicated primers (supplemental Table S1) using the Step One Real-time PCR system (Applied Biosystems).

Immunoblotting—Cells were lysed in lysis buffer (20 mM Tris-HCl, pH 7.4) containing 150 mM NaCl, 1% Nonidet P-40,

10 mM EDTA, 25 mM iodoacetamide, 2 mM PMSF and a protease inhibitor mixture (Roche Applied Science). Lysates were clarified by centrifugation and subjected to SDS-PAGE (10% gel) under reducing conditions, followed by immunoblotting with anti-Raftlin pAb or anti-β actin mAb.

Immunoprecipitation—HeLa cells were stimulated with 40 μg/ml of poly(I:C) for 30 min at 37 °C. At timed intervals, cells were lysed in lysis buffer for 30 min on ice. Lysates were precleared with protein G-Sepharose (GE Healthcare) and incubated with 1 μg of anti-clathrin heavy chain mAb. Immunocomplexes were recovered by incubation with Protein G-Sepharose, washed once with lysis buffer, and resuspended in denaturing buffer. Samples were analyzed by SDS-PAGE (10% gel) under reducing conditions, followed by immunoblotting with anti-Raftlin pAb (1:1000) and HRP-conjugated secondary Ab. The membrane was re-probed with anti-clathrin heavy chain mAb (1:400).

Confocal Microscopy—HeLa cells (1×10^5 cells/well) were plated onto micro coverglasses (Matsunami Glass) in 12-well plates. The next day, cells were incubated with 40 μg/ml of poly(I:C) for 30 min at 4 °C. Cells were washed once and further incubated for 5–30 min at 37 °C. At timed intervals, cells were fixed with 4% paraformaldehyde for 30 min and permeabilized with PBS containing 0.5% saponin and 1% BSA for 30 min. Fixed cells were blocked in PBS containing 1% BSA and labeled with anti-Raftlin pAb (1:500), anti-human TLR3 mAb (20 μg/ml), or Alexa Fluor 488-CTXB (10 μg/ml) for 60 min at room temperature. Alexa Fluor 488- or Alexa Fluor 568-conjugated secondary Abs (1:400) were used to visualize the primary Abs. Nuclei were stained with DAPI (2 μg/ml) in PBS for 10 min before mounting onto glass slides using PBS containing 2.3% DABCO and 50% glycerol. Cells were visualized at a ×63 magnification with an LSM510 META microscope (Zeiss, Jena, Germany).

For uptake study, HeLa cells or HEK293 cells transfected with control siRNA or siRNA for Raftlin were incubated with 40 μg/ml of Texas Red/poly(I:C), Alexa Fluor 568/transferrin (25 μg/ml), or FITC/ODN2006 (40 μg/ml) for 30 min at 4 °C. After washing, cells were further incubated at 37 °C. At timed intervals, fixed cells were visualized as described above. In the case of HEK293 cells, cells (1×10^5 cells/well) were plated onto poly-L-lysine-coated glass (BD Bioscience) in a 24-well plate and cultured for 12 h.

Control or Raftlin knockdown MoDCs (2×10^5/100 μl) were incubated with 40 μg/ml of Texas Red/poly(I:C) for 30 min at 4 °C, washed once, and then incubated for 5–30 min at 37 °C. At timed intervals, cells were fixed with 4% paraformaldehyde for 15 min and centrifuged by Cytospin3 (Shandon). After mounting with ProLong Gold with DAPI (Molecular Probes), cells were visualized by confocal microscopy. In some experiments, MoDCs were pretreated with 1 mM MβCD for 1 h at 37 °C. Viability of cells treated with MβCD was 93.3%. For staining of endosomes, fixed cells were permeabilized with PBS containing 0.5% saponin and 1% BSA for 30 min (staining of TLR3 and early endosome), or PBS containing 100 μg/ml of digitonin and 1% BSA for 30 min (staining of late endosome). After blocking, cells were labeled with anti-Raftlin pAb (1:500), anti-human TLR3 mAb (20 μg/ml), anti-Rab5 mAb (4 μg/ml), or anti-LAMP1 mAb (H4A3) (1:200) for 60 min at room temperature.

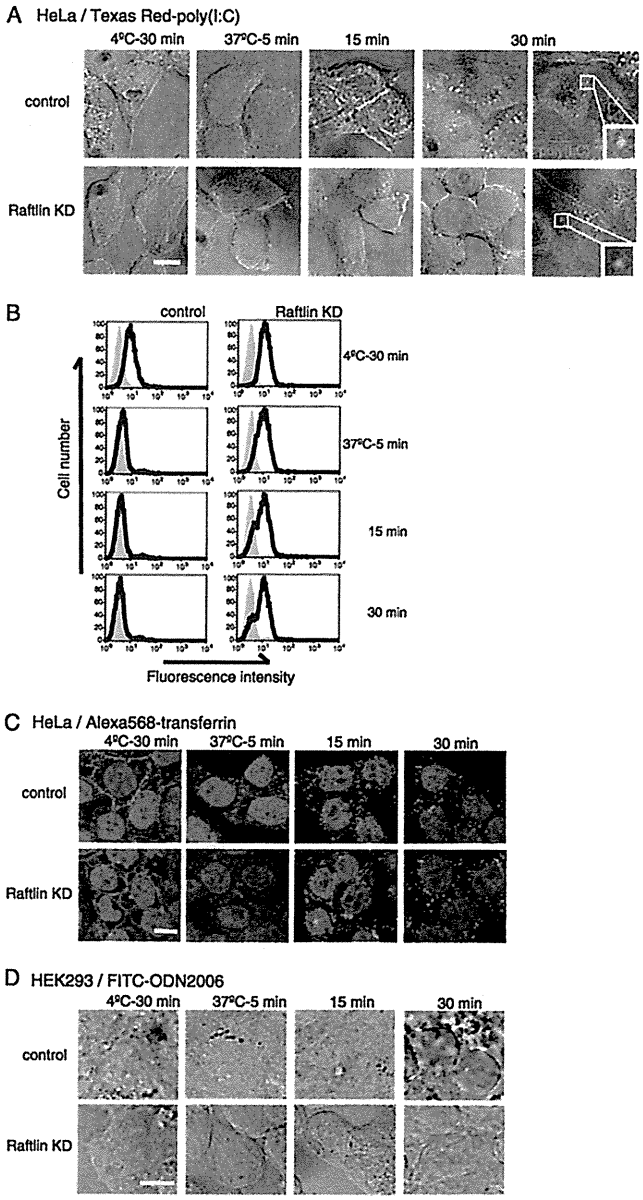

FIGURE 3. **Knockdown of Raftlin suppresses cellular uptake of poly(I:C) and B-type ODN but not transferrin.** HeLa cells (*A* and *C*) and HEK293 cells (*D*) were transfected with control siRNA (*upper panels*) or siRNA for Raftlin (*lower panels*). Forty-eight hours after transfection, cells were washed and incubated with 40 μg/ml of Texas Red/poly(I:C) (*A*), 25 μg/ml Alexa Fluor 568/transferrin (*C*), or 40 μg/ml of FITC/ODN2006 (*D*) for 30 min at 4 °C. After washing, cells were incubated for up to 30 min at 37 °C. At timed intervals, cells were fixed and visualized by confocal microscopy. In some experiments, cells were fixed or permeabilized and stained with anti-TLR3 mAb. *A, red,* Texas Red-poly(I:C); *green,* TLR3. *C, red,* Alexa 568/transferrin; *blue,* nuclei with DAPI. *D, green,* FITC/ODN2006. *Bar,* 10 μm. *B,* flow cytometric analysis of poly(I:C) uptake. Control and Raftlin knockdown HeLa cells were incubated with 20 μg/ml of poly(I:C) for 30 min at 4 °C. After washing, cells were incubated for up to 30 min at 37 °C. At the indicated time points, cells were labeled with anti-dsRNA mAb (*black lines*) or mouse IgG2a (*shaded histogram*) and FITC-labeled secondary Ab. The cells were analyzed on a FACS Calibur.

Flow Cytometry—Cells were incubated with the indicated concentrations of poly(I:C) in culture medium for 30 min at 4 °C. After washing, cells were labeled with anti-dsRNA mAb

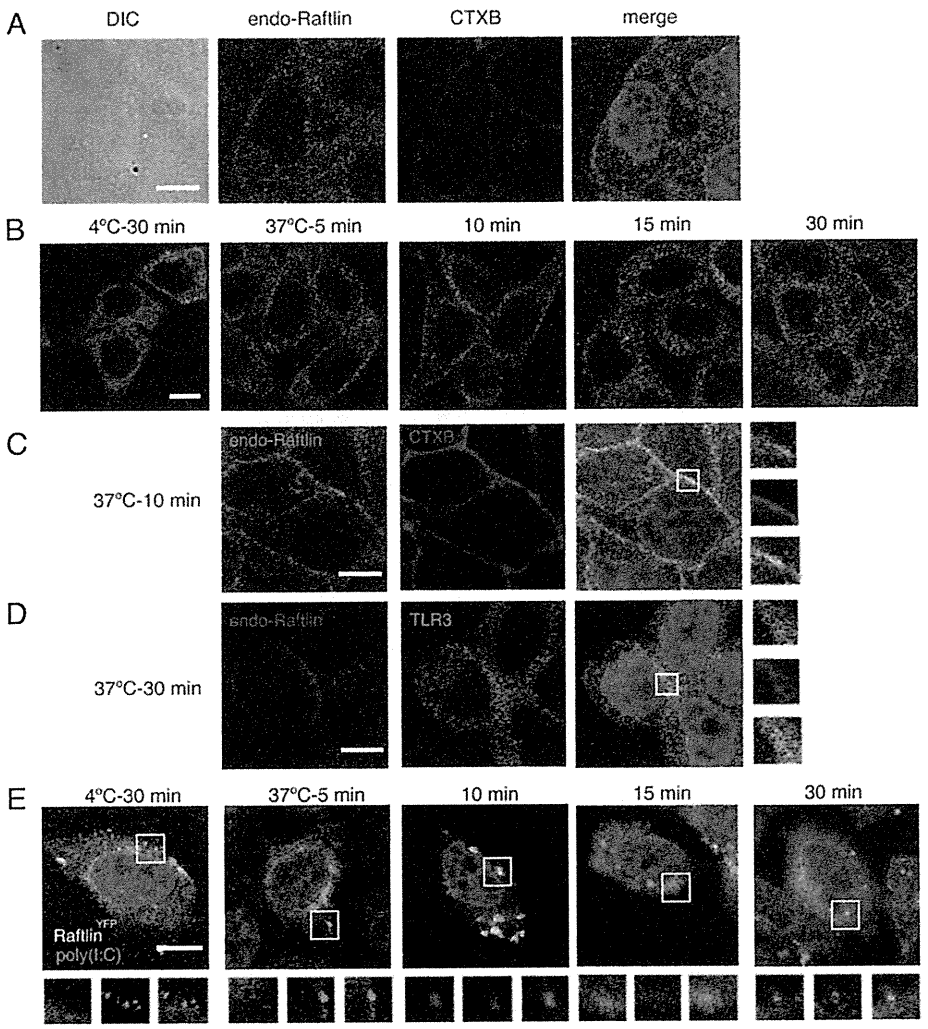

FIGURE 4. **Translocation of Raftlin in response to poly(I:C).** *A*, confocal images of endogenous Raftlin in HeLa cells. Fixed and permeabilized cells were stained with anti-Raftlin pAb and Alexa Fluor 488/CTXB. *Red*, endogenous Raftlin; *green*, CTXB; *blue*, nuclei with DAPI. *Bar*, 10 μm. *B–D*, spatiotemporal mobilization of endogenous Raftlin in response to poly(I:C). HeLa cells were incubated with 40 μg/ml of poly(I:C) as described in the legend to Fig. 3. At the indicated periods, cells were fixed and stained with anti-Raftlin pAb (*B*), anti-Raftlin pAb and Alexa Fluor 488/CTXB (*C*), or anti-Raftlin pAb and anti-TLR3 mAb (*D*). Representative data from the indicated time points are shown. *B* and *C*, *red*, endogenous Raftlin; *green*, Alexa 488/CTXB. *D*, *green*, endogenous Raftlin; red, TLR3; *blue*, nuclei with DAPI. *Bar*, 10 μm. *E*, association of Raftlin with poly(I:C). Confocal images of poly(I:C) uptake by HeLa cells expressing Raftlin^{YFP}. HeLa cells were transfected with Raftlin^{YFP} and incubated with 40 μg/ml of Texas Red/poly(I:C) as described above. At the indicated periods, cells were fixed and visualized by confocal microscopy. *Lower panels* show ×2 magnified images of the *insets* in the *upper panels*. *Yellow*, Raftlin^{YFP}; *red*, Texas Red/poly(I:C); *blue*, nuclei with DAPI. *Bar*, 10 μm.

(K1) or mouse IgG2a as a control (1 μg) in the presence of human IgG (10 μg) for 30 min at 4 °C in FACS buffer (Dulbecco's phosphate-buffered saline containing 0.5% BSA and 0.1% sodium azide) and then incubated with FITC-labeled secondary Ab. Cells were analyzed on a FACS Calibur flow cytometer (BD Biosciences).

Statistical Analysis—Statistical significance of differences between groups was determined by the Student's *t* test.

RESULTS

Raftlin Participates in Poly(I:C)-induced TLR3-mediated Signaling—We previously demonstrated that poly(I:C) binds to human MoDCs and HEK293 cells (27). Because poly(I:C) also activates B cells (32), we screened B cell lines capable of binding poly(I:C) and found that Raji cells bound poly(I:C) at an equivalent level to MoDCs (supplemental Fig. S1). To identify the proteins involved in poly(I:C) cellular uptake, we isolated the poly(I:C)-binding proteins from Raji cell lysates by sequential affinity chromatography using Sepharose, poly(U)-Sepharose, and poly(I:C)-Sepharose. The eluate from poly(U)- or poly(I:C)-Sepharose was subjected to SDS-PAGE, followed by mass spectrometric analyses. A total of 127 proteins were identified, which preferentially bound to poly(I:C)-Sepharose rather than to poly(U)-Sepharose (supplemental Table S2). They included several proteins with a dsRNA-binding motif, such as interferon-induced dsRNA-activated protein kinase (supplemental Table 3). Also, clathrin heavy chain 1 and several cytoskeleton molecules, such as tubulin and actinin-1, were identified, suggesting that poly(I:C) uptake machinery might be isolated from the cell lysates as a complex. In the membrane/cytoskeleton group, only four are membrane-associated proteins (supplemental Table S3). We selected transmembrane proteins LYRIC

(also called Astrocyte elevated gene 1) and 4F2 cell surface antigen heavy chain (4F2, also named CD98), and a cytoplasmic protein Raftlin that contains a membrane-anchoring motif at the N terminus. Because HEK293 cells express these molecules, we first examined whether they are involved in poly(I:C)-induced TLR3-mediated signaling by gene silencing. As a positive control, knockdown of TICAM-1 was performed. Interestingly, poly(I:C)-induced TLR3-mediated IFN-β promoter activation was greatly reduced when Raftlin was knocked down in HEK293 cells, whereas silencing of the LYRIC or 4F2 genes did not affect poly(I:C) function (Fig. 1*A*, *left-hand panel*). Poly(I:C)-induced TLR3-mediated NF-κB activation was also decreased in Raftlin knockdown HEK293 cells, in a similar way to TICAM-1 knockdown cells (Fig. 1*B*). In contrast, TLR2-mediated NF-κB activation was substantially induced in all cells subjected to gene silencing (Fig. 1*C*). The failure of IFN-β promoter activation in Raftlin knockdown HEK293 cells was also observed when cells were stimulated with increasing amounts of poly(I:C) (Fig. 1*D*). These results strongly suggest that Raftlin participates in poly(I:C)-induced TLR3 activation.

Raftlin Is Essential for Poly(I:C)-induced IFN-β Production in HeLa Cells—Raftlin was originally identified as a major lipid raft protein required for lipid raft integrity, B cell receptor signal transduction, and modulation of T cell receptor signaling (29, 33). We analyzed the expression of Raftlin and Raftlin-2, a homologue of Raftlin, in HEK293, HeLa, and Raji cells by RT-PCR. As shown in Fig. 2*A*, these cell lines express Raftlin but not Raftlin-2 mRNA. The protein expression level of Raftlin was further examined by immunoblotting with an anti-human Raftlin pAb (29). Raftlin was abundantly expressed in Raji cells, and expressed at lower levels in HEK293 and HeLa cells (Fig. 2*B*). Poly(I:C)-induced IFN-β mRNA expression was greatly diminished by knockdown of Raftlin in HeLa cells, in a similar way to TICAM-1 knockdown. In contrast, HeLa cells transfected with siRNA for 4F2 or LYRIC efficiently responded to poly(I:C) (Fig. 2*C*, *left-hand panel*, and supplemental Fig. S2). The expression of TLR3, TICAM-1, MDA5, and IPS-1 was not affected by knockdown of Raftlin (Fig. 2*D*). Thus, Raftlin plays a critical role in poly(I:C)-induced IFN-β production.

Raftlin Is Indispensable for Poly(I:C) Cellular Uptake—To examine the role of Raftlin in poly(I:C)-induced cellular responses, we analyzed cell entry of poly(I:C) in Raftlin knockdown HeLa cells. Texas Red-labeled poly(I:C), whose biological activity was similar to that of unlabeled poly(I:C) (supplemental Fig. S3), unevenly bound to the cell surface of HeLa cells either transfected with control siRNA or Raftlin siRNA after 30 min incubation at 4 °C (Fig. 3*A*, *left panels*). When the incubation condition was changed to 37 °C for 5 min, poly(I:C) was detected as speckles at the cell surface in both cells, although some of the poly(I:C) was internalized in control cells (*second set of panels*). However, after 15 min, poly(I:C) localized diffusely in the endosomal compartments in control cells, whereas it still resided on the cell surface as speckles in Raftlin knockdown cells (*third set of panels*). Thus, clustering of the uptake receptor occurs without internalization in Raftlin knockdown cells. After 30 min, poly(I:C) accumulated in the endosomal compartments in control cells, where it colocalized with TLR3 (Fig. 3*A*, *upper right panel*). In contrast, Raftlin knockdown

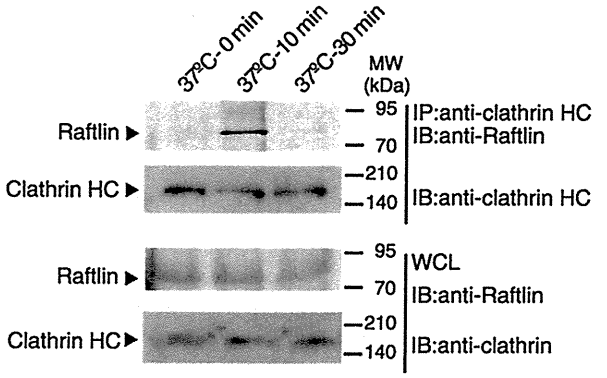

FIGURE 5. **Raftlin associates with clathrin in response to poly(I:C).** HeLa cells were stimulated with 40 μg/ml of poly(I:C) for 0–30 min at 37 °C. At timed intervals, cells were lysed in lysis buffer and clathrin was immunoprecipitated (*IP*) using an anti-clathrin heavy chain (*HC*) mAb. The immunoprecipitants were resolved on SDS-PAGE (10% gel) under reducing conditions followed by immunoblotting (*IB*) with anti-Raftlin pAb or anti-clathrin HC mAb. Whole cell lysates (*WCL*) were subjected to immunoblotting with anti-Raftlin pAb or anti-clathrin HC mAb to detect endogenous protein expression. Molecular mass markers are indicated on the *right*.

HeLa cells did not permit cell entry of poly(I:C). Consistent with these results, flow cytometric analysis showed that surface poly(I:C) disappeared in control but not in Raftlin knockdown HeLa cells (Fig. 3*B*). After a 30-min incubation at 37 °C, poly(I:C) was detected on the cell surface of ~80% of HeLa cells transfected with Raftlin-siRNA, which reflects the knockdown efficiency.

Because poly(I:C) is internalized into cells by the clathrin-dependent endocytic pathway, we examined whether uptake of transferrin, which occurs in a clathrin-dependent manner, is suppressed by Raftlin knockdown. As shown in Fig. 3*C*, transferrin was internalized into HeLa cells irrespective of Raftlin knockdown. We previously reported that B- and C-type ODNs share their uptake receptor with poly(I:C) in HEK293 cells and MoDCs and are delivered to TLR3-positive endosomes in MoDCs (27). Indeed, FITC-labeled B-type ODN (ODN 2006) failed to enter cells when Raftlin was silenced in HEK293 cells (Fig. 3*D*). These results indicate that Raftlin is essential for uptake of poly(I:C) and B- and C-type ODNs via receptor-mediated endocytosis.

Raftlin Is Involved in the Uptake Machinery for Poly(I:C)—A previous study showed that Raftlin is localized exclusively in lipid rafts by fatty acylation of the N-terminal Gly-2 and Cys-3 residues in human B cells (29). We analyzed the subcellular localization of Raftlin in HeLa cells. Endogenous Raftlin was localized diffusely in the cytoplasm and did not merge with CTXB, which binds to the lipid raft molecule GM1, suggesting the cell type-dependent localization of Raftlin (Fig. 4*A*). We next examined the translocation of Raftlin in response to poly(I:C). At the poly(I:C) binding step (4 °C, 30 min), Raftlin resided in the cytoplasm (Fig. 4*B*, *left panel*). After a 5-min incubation at 37 °C, most of the Raftlin remained localized in the cytoplasm. However, after 10 min, membrane-associated Raftlin was observed, which partially colocalized with CTXB (Fig. 4, *B*, *third panel*, and *C*). Interestingly, Raftlin transferred to the endosomal structures from the plasma membrane within 15 min, and colocalized with TLR3 after 30 min of incubation (Fig. 4*D*).

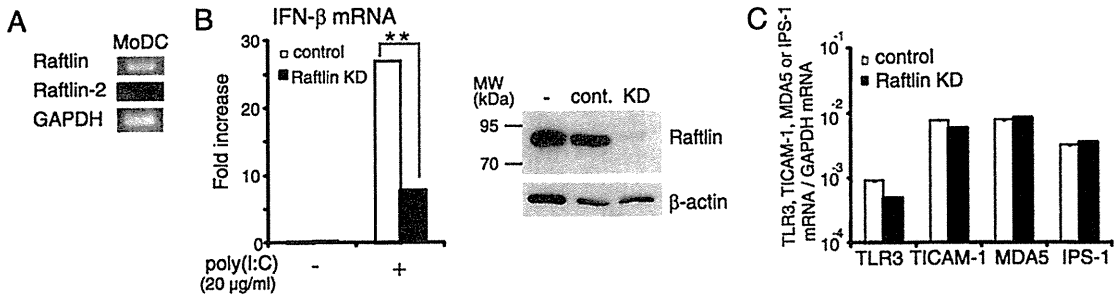

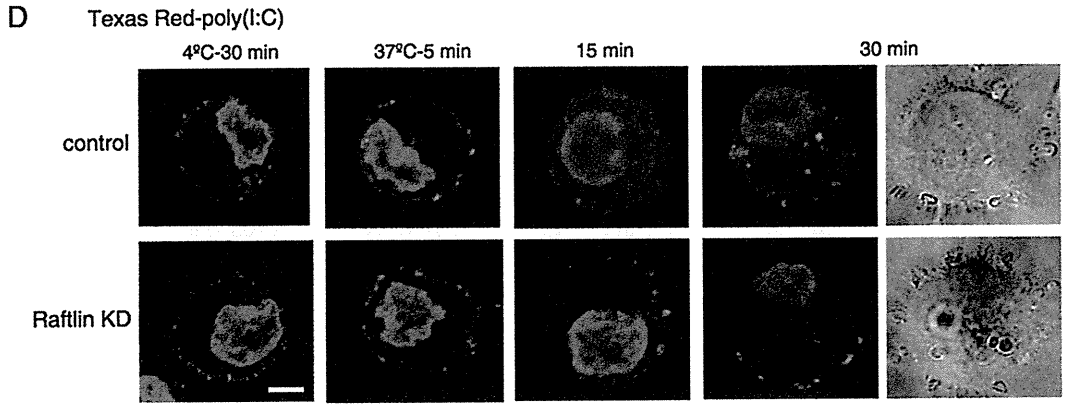

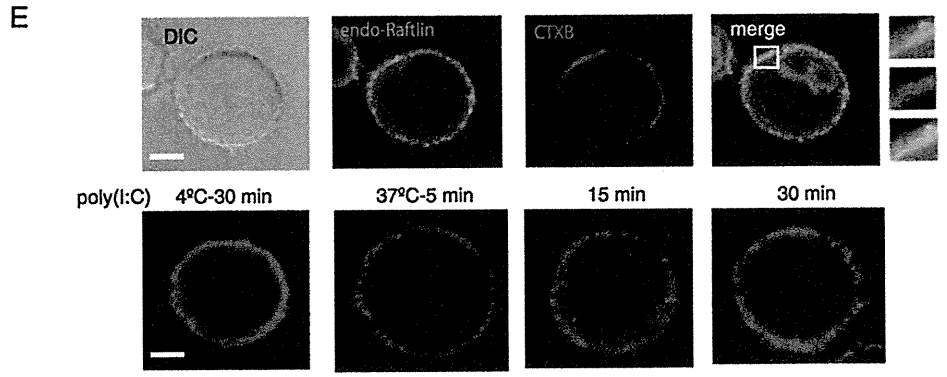

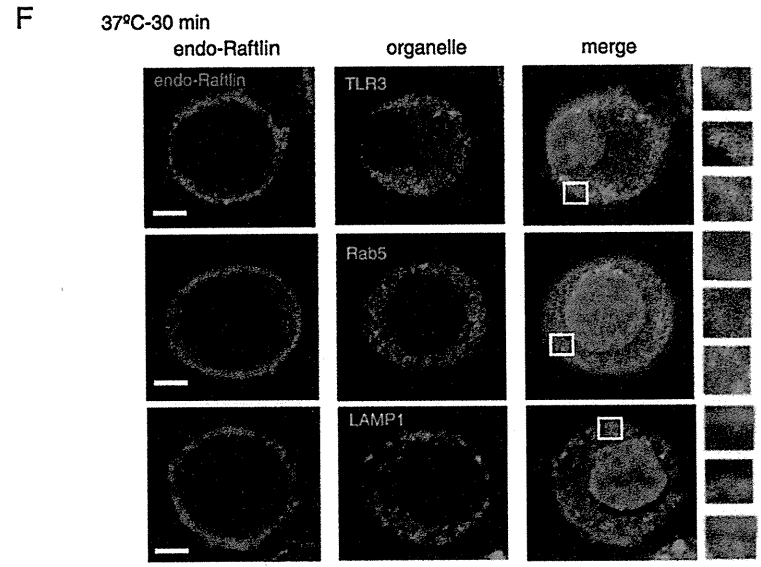

To visualize the spatiotemporal mobilization of Raftlin and poly(I:C), HeLa cells were transfected with the expression vector for Raftlin^{YFP} and incubated with Texas Red-labeled poly(I:C). The subcellular localization and translocation of Raftlin^{YFP} in response to poly(I:C) were almost similar to those observed with endogenous Raftlin (Fig. 4*E*). Notably, Raftlin^{YFP} co-localized with Texas Red-poly(I:C) at the plasma membrane after 10-min incubation at 37 °C. Thereafter, poly(I:C) was internalized, spread to the endosomal compartments, and then accumulated in the organelles as shown in Fig. 3*A*. A membrane-associated Raftlin^{YFP} appeared to move along with internalized poly(I:C) (Fig. 4*E*).

To clarify the function of Raftlin in poly(I:C) internalization mediated by clathrin, we examined physical association of Raftlin with clathrin. As shown in Fig. 5, Raftlin did not interact with clathrin in unstimulated HeLa cells. When cells were stimulated with poly(I:C), Raftlin was co-immunoprecipitated with clathrin after a 10-min stimulation. However, after 30 min, Raftlin did not interact with clathrin any more. These results suggest that after poly(I:C) binding to the uptake receptor, Raftlin was recruited to the plasma membrane and associates with the clathrin complex to modulate cargo sorting and delivery.

Raftlin Is Critical for Poly(I:C)-induced IFN-β Production in Human Myeloid DCs—Human MoDCs expressed Raftlin but not Raftlin-2 mRNA (Fig. 6*A*). When DCs were electrically transfected with siRNA for Raftlin, Raftlin expression was decreased compared with cells transfected with control siRNA (Fig. 6*B*, *right-hand panel*). Poly(I:C)-induced IFN-β mRNA expression was diminished in the Raftlin knockdown DCs (Fig. 6*B*, *left-hand panel*). The mRNA expression levels of TICAM-1, MDA5, and IPS-1 in Raftlin knockdown DCs were comparable with those in control DCs, although TLR3 expression was slightly reduced compared with control cells (Fig. 6*C*). Again, entry of poly(I:C) into Raftlin knockdown DCs was inhibited (Fig. 6*D*).

Raftlin was localized to both the plasma membrane and the cytoplasm of DCs (Fig. 6*E*, *upper panels*). Although membrane-associated Raftlin partially colocalized with CTXB, lipid raft disruption with MβCD in DCs did not affect poly(I:C) cellular uptake (supplemental Fig. S4). The mobilization of Raftlin in response to poly(I:C) was similar to that observed in HeLa cells (Fig. 6*E*, *lower panels*). After 30 min, Raftlin colocalized with TLR3 and Rab5 but not with LAMP1, indicating that Raftlin, together with the poly(I:C) uptake receptor, moves from the plasma membrane to the TLR3-positive early endosomes (Fig. 6*F*).

To determine the physiological function of Raftlin, we analyzed poly(I:C)-induced IFN-β production by BMDCs from wild-type or Raftlin$^{-/-}$ mice. Remarkably, wild-type and Raftlin$^{-/-}$ BMDCs expressed mouse Raftlin-2 mRNA at equivalent levels (Fig. 7*A*). There was no significant difference in poly(I:C)-induced IFN-β production between wild-type and Raftlin$^{-/-}$ BMDCs (Fig. 7*B*). In addition, cellular uptake of poly(I:C) in Raftlin$^{-/-}$ BMDCs was comparable with that in wild-type BMDCs (Fig. 7*C*). To test the possibility that the Raftlin function is compensated with Raftlin-2 in Raftlin$^{-/-}$ BMDCs as observed in B cell receptor signaling in Raftlin$^{-/-}$ mouse B cells (33), we knocked down of mouse Raftlin-2 in Raftlin$^{-/-}$ BMDCs by infection with Raftlin-2 shRNA-expressing lentiviral particles and analyzed the cellular response to poly(I:C). Mouse Raftlin-2 expression was partially decreased in Raftlin$^{-/-}$ BMDCs (Fig. 7*D*, *right-hand panel*). Poly(I:C)-induced IFN-β mRNA expression was partially but significantly decreased in Raftlin-2 knockdown Raftlin$^{-/-}$ BMDCs (Fig. 7*D*, *left-hand panel*). Furthermore, internalization of Texas Red-labeled poly(I:C) was inhibited in ~40% of Raftlin$^{-/-}$ BMDCs infected with mouse Raftlin-2 shRNA lentiviral particles, reflecting the knockdown efficiency of mouse Raftlin-2 (Fig. 7*E*). These results suggest that mouse Raftlin-2 participates in poly(I:C) cellular uptake in Raftlin$^{-/-}$ BMDCs.

DISCUSSION

Recent studies using mouse implanted tumor models indicate that poly(I:C) is a promising adjuvant for tumor vaccines because it promotes adaptive anti-tumor responses through the activation of myeloid DCs and induction of type I IFN production by multiple type of cells (10–15). However, it remains unresolved how poly(I:C) is delivered from the extracellular fluid to the intracellular poly(I:C) sensors localized on the endosomal membrane or cytoplasm.

In this study, we demonstrated that Raftlin is essential for poly(I:C)-induced cellular responses in human myeloid DCs and epithelial cells by mediating the cellular uptake of poly(I:C). Raftlin was originally identified as a major raft protein in B cells that co-localized with B cell receptor in the lipid raft before and after B cell receptor stimulation (29). However, subcellular localization of endogenous Raftlin appears to depend on the cell types. We found that in unstimulated HeLa cells, endogenous Raftlin localized diffusely in the cytoplasm and did not co-

FIGURE 6. **Raftlin is critical for poly(I:C)-induced IFN-β production in human myeloid DCs.** *A*, MoDCs express Raftlin but not Raftlin-2 mRNA. *B*, poly(I:C)-induced IFN-β production was decreased in Raftlin knockdown DCs (*left-hand panel*). Control and Raftlin knockdown DCs in a 24-well plate (7×10^5/ml) were stimulated with 20 μg/ml of polymyxin B-treated poly(I:C) for 4 h. Total RNA was extracted and subjected to RT qPCR analysis for the expression of IFN-β. Data are representative of three separate experiments with similar results (mean ± S.D.). **, $p < 0.01$. Protein expression of Raftlin in DCs (4×10^5) before and after siRNA transfection is shown (*B*, *right panel*). *C*, expression of TLR3, TICAM-1, MDA5, and IPS-1 in DCs. Total RNA from control and Raftlin knockdown DCs were extracted and subjected to RT-qPCR analysis for the expression of mRNA. Expression of each gene was normalized to GAPDH mRNA expression. *D*, uptake of Texas Red/poly(I:C) by MoDCs transfected with control siRNA (*upper panels*) or siRNA for Raftlin (*lower panels*). Control or Raftlin knockdown DCs were incubated with 40 μg/ml of Texas Red/poly(I:C) for 30 min at 4 °C. After washing, cells were incubated for up to 30 min at 37 °C. At the indicated periods, cells were fixed and visualized by confocal microscopy. Representative images from 20 fields in the indicated time points are shown. *Red*, Texas Red/poly(I:C); *blue*, nuclei with DAPI. *Bar*, 5 μm. *E* and *F*, confocal images of endogenous Raftlin in MoDCs in response to poly(I:C). *E*, *upper panels*, DCs were fixed and stained with anti-Raftlin pAb and Alexa 488/CTXB. *Red*, endogenous Raftlin; *green*, Alexa 488/CTXB; *blue*, nuclei with DAPI. *E*, *lower panels*, and *F*, DCs were incubated with 40 μg/ml of poly(I:C) as described in the legend to Fig. 4. At the indicated periods, cells were fixed and stained with anti-Raftlin pAb, anti-TLR3 mAb, anti-Rab5 mAb, or anti-LAMP1 mAb and Alexa Fluor-conjugated secondary Abs. Representative data from the indicated time points are shown. *Green*, endogenous Raftlin; *red*, TLR3, Rab5, or LAMP-1; *blue*, nuclei with DAPI. *Bar*, 5 μm.

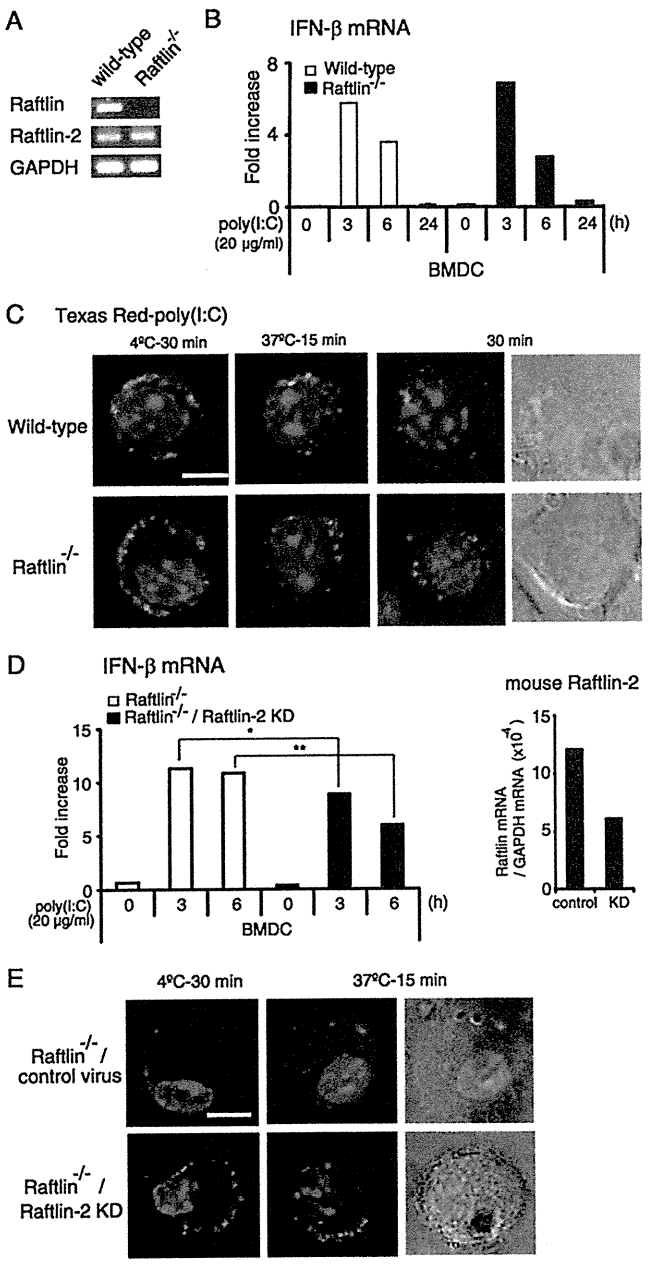

FIGURE 7. **Poly(I:C) uptake and IFN-β production by Raftlin$^{-/-}$ BMDCs.** *A*, expression of Raftlin and Raftlin-2 mRNAs in BMDCs from wild-type or Raftlin$^{-/-}$ mice. *B*, IFN-β mRNA expression in BMDCs from wild-type or Raftlin$^{-/-}$ mice in response to poly(I:C). Cells were stimulated with 20 μg/ml of polymyxin B-treated poly(I:C). At the indicated time points, cells were washed and total RNA was extracted. RT qPCR was performed using the primers for mouse IFN-β. Data (mean ± S.D.) are representative of three separate experiments with similar results. *C*, BMDCs from wild-type (*upper panels*) or Raftlin$^{-/-}$ mice (*lower panels*) were incubated with 40 μg/ml of Texas Red/poly(I:C) for 30 min at 4 °C. After washing, cells were incubated for up to 30 min at 37 °C. At timed intervals, cells were fixed and visualized by confocal microscopy. Representative images from 20 fields in the indicated time points are shown. *Red*, Texas Red/poly(I:C); *blue*, nuclei with DAPI. *Bar*, 5 μm. *D*, poly(I:C)-induced IFN-β mRNA expression in control and Raftlin-2 knockdown Raftlin$^{-/-}$ BMDCs. *Left-hand panel*, control and Raftlin-2 knockdown Raftlin$^{-/-}$ BMDCs were stimulated with 20 μg/ml of polymyxin B-treated poly(I:C). At the indicated time points, IFN-β mRNA expression was analyzed as described above. *Right-hand panel*, mouse Raftlin-2 mRNA expression. Representative data from two independent experiments are shown. *, $p < 0.05$; **, $p < 0.01$. *E*, poly(I:C) cellular uptake by control and Raftlin-2 knockdown Raftlin$^{-/-}$ BMDCs. Representative images from 20 fields in the indicated time points are shown. In Raftlin$^{-/-}$ BMDCs infected with mouse Raftlin-2 shRNA lentiviral particles, 40% of cells fail to internalize poly(I:C) after a 15-min incubation at 37 °C. The number of cells lacking Texas Red/poly(I:C) internalization/total number of cells were for control Raftlin$^{-/-}$ BMDCs, 0/137, and Raftlin-2 knockdown Raftlin$^{-/-}$ BMDCs, 106/260. *Red*, Texas Red/poly(I:C); *blue*, nuclei with DAPI. *Bar*, 5 μm.

localize with CTXB (Fig. 4), whereas in MoDCs it localized to both the plasma membrane and the cytoplasm and membrane-associated Raftlin partially merged with CTXB (Fig. 6*E*). In these cells, poly(I:C) stimulation induced the translocation of Raftlin from the cytoplasm to the plasma membrane where it cooperated with uptake receptor to deliver poly(I:C) to TLR3-positive endosomes (Figs. 4 and 6*F*). Thus, Raftlin is involved in the nucleocapture complex triggering poly(I:C)-mediated TLR3 activation, and appears to act downstream of immune receptors in a cell type-specific manner.

Notably, Raftlin$^{-/-}$ BMDCs that express Raftlin-2 normally took up poly(I:C) (Fig. 7*C*). The expression of Raftlin or Raftlin-2 depends on the cell type. Mouse Raftlin-2 is expressed in B cells but not T cells and is thought to function in a similar way to Raftlin in mouse B cells (33). Because poly(I:C)-induced IFN-β mRNA expression and internalization of poly(I:C) were decreased when mouse Raftlin-2 was knocked down in Raftlin$^{-/-}$ BMDCs (Fig. 7, *D* and *E*), mouse Raftlin-2 participates in poly(I:C) uptake in Raftlin$^{-/-}$ BMDCs. In humans, MoDCs, HEK293 cells, and HeLa cells did not express Raftlin-2 mRNA. Hence, human Raftlin plays a key role in poly(I:C)-induced cellular responses in the absence of Raftlin-2.

The molecular mechanism by which Raftlin cooperates with the uptake receptor to mediate cell entry of poly(I:C) and B- and C-type ODNs is currently unknown. As shown in Fig. 3*A*, clustering of the uptake receptor occurs without internalization in the absence of Raftlin. Because disruption of the lipid raft by treatment with MβCD did not affect internalization of poly(I:C) (supplemental Fig. S4), Raftlin may participate in the assembly of the uptake machinery for poly(I:C) and B- and C-type ODNs independently of lipid raft function. We have previously demonstrated that poly(I:C) is internalized via the clathrin-mediated endocytosis (27). Indeed, Raftlin associated with clathrin after poly(I:C) stimulation (Fig. 5). Thus, Raftlin might be involved in the clathrin and clathrin-associated adapter protein complexes at the plasma membrane and participates in cargo sorting and delivery to the TLR3-positive endosome (34).

Intriguingly, A-type ODN that activates plasmacytoid DCs to induce IFN-α was unable to bind to myeloid DCs (27). A-type ODN binds to high mobility group box 1 and augments the binding of high mobility group box 1 to receptor for advanced glycation end products (35). A-type ODN-high mobility group box 1 complex enhances TLR9-mediated IFN-α production by plasmacytoid DCs in a receptor for advanced glycation end product-dependent manner, although receptor for advanced glycation end products is not essential for internalization of A-type ODN or A-type ODN-high mobility group box 1 complexes. An unidentified uptake receptor for A-type ODN must reside on plasmacytoid DCs. Although whether Raftlin participates in the uptake of A-type ODN in human plasmacytoid DCs remains to be examined, we surmise that exogenous

nucleic acids are recognized by cell surface receptors that form distinct nucleocapture complexes to deliver nucleic acids to intracellular organelles.

The adjuvant activity of poly(I:C) is derived from the activation of two innate immune sensors, TLR3 and MDA5, in myeloid DCs. No RNA molecule has been reported besides poly(I:C) that extracellulary activates either TLR3 or MDA5. Identification of the uptake receptor for poly(I:C) in DCs is important to elucidate the mechanism by which poly(I:C) is localized to TLR3 and MDA5, as well as to develop a poly(I:C)-related adjuvant that is selectively transferred to TLR3 and/or MDA5.

Acknowledgments—We thank Dr. Y. Miyamoto and K. Shida (Osaka Medical Center for Cancer, Osaka, Japan) for technical support and Drs. H. Oshiumi, T. Ebihara, H. Takaki, H. H. Aly, and J. Kasamatsu for invaluable discussions. We also thank Dr. J. P. Atkinson (Washington University) for reviewing this manuscript.

REFERENCES

1. Nagano, Y., and Kojima, Y. (1954) *Compt. Pend. Soc. Biol.* **148,** 1700–1702
2. Lindenmann, J., Burke, D. C., and Isaacs, A. (1957) *Br. J. Exp. Pathol.* **38,** 551–562
3. Field, A. K., Tytell, A. A., Lampson, G. P., and Hilleman, M. R. (1967) *Proc. Natl. Acad. Sci. U.S.A.* **58,** 1004–1010
4. Alexopoulou, L., Holt, A. C., Medzhitov, R., and Flavell, R. A. (2001) *Nature* **413,** 732–738
5. Matsumoto, M., Kikkawa, S., Kohase, M., Miyake, K., and Seya, T. (2002) *Biochem. Biophys. Res. Commun.* **293,** 1364–1369
6. Yoneyama, M., Kikuchi, M., Matsumoto, K., Imaizumi, T., Miyagishi, M., Taira, K., Foy, E., Loo, Y. M., Gale, M., Jr., Akira, S., Yonehara, S., Kato, A., and Fujita, T. (2005) *J. Immunol.* **175,** 2851–2858
7. Kato, H., Takeuchi, O., Sato, S., Yoneyama, M., Yamamoto, M., Matsui, K., Uematsu, S., Jung, A., Kawai, T., Ishii, K. J., Yamaguchi, O., Otsu, K., Tsujimura, T., Koh, C. S., Reis e Sousa, C., Matsuura, Y., Fujita, T., and Akira, S. (2006) *Nature* **441,** 101–105
8. Gitlin, L., Barchet, W., Gilfillan, S., Cella, M., Beutler, B., Flavell, R. A., Diamond, M. S., and Colonna, M. (2006) *Proc. Natl. Acad. Sci. U.S.A.* **103,** 8459–8464
9. Schultz, O., Diebold, S. S., Chen, M., Näslund, T. I., Nolte, M. A., Alexopoulou, L., Azuma, Y. T., Flavell, R. A., Liljeström, P., and Reis e Sousa, C. (2005) *Nature* **433,** 887–892
10. Matsumoto, M., and Seya, T. (2008) *Adv. Drug Deliv. Rev.* **60,** 805–812
11. Kumar, H., Koyama, S., Ishii, K. J., Kawai, T., and Akira, S. (2008) *J. Immunol.* **180,** 683–687
12. McCartney, S., Vermi, W., Gilfillan, S., Cella, M., Murphy, T. L., Schreiber, R. D., Murphy, K. M., and Colonna, M. (2009) *J. Exp. Med.* **206,** 2967–2976
13. Miyake, T., Kumagai, Y., Kato, H., Guo, Z., Matsushita, K., Satoh, T., Kawagoe, T., Kumar, H., Jang, M. H., Kawai, T., Tani, T., Takeuchi, O., and Akira, S. (2009) *J. Immunol.* **183,** 2522–2528
14. Longhi, M. P., Trumpfheller, C., Idoyaga, J., Caskey, M., Matos, I., Kluger, C., Salazar, A. M., Colonna, M., and Steinman, R. M. (2009) *J. Exp. Med.* **206,** 1589–1602
15. Ebihara, T., Azuma, M., Oshiumi, H., Kasamatsu, J., Iwabuchi, K., Matsumoto, K., Saito, H., Taniguchi, T., Matsumoto, M., and Seya, T. (2010) *J. Exp. Med.* **207,** 2675–2687
16. Matsumoto, M., Funami, K., Tanabe, M., Oshiumi, H., Shingai, M., Seto, Y., Yamamoto, A., and Seya, T. (2003) *J. Immunol.* **171,** 3154–3162
17. Funami, K., Sasai, M., Ohba, Y., Oshiumi, H., Seya, T., and Matsumoto, M. (2007) *J. Immunol.* **179,** 6867–6872
18. Oshiumi, H., Matsumoto, M., Funami, K., Akazawa, T., and Seya, T. (2003) *Nat. Immunol.* **4,** 161–167
19. Yamamoto, M., Sato, S., Hemmi, H., Hoshino, K., Kaisho, T., Sanjo, H., Takeuchi, O., Sugiyama, M., Okabe, M., Takeda, K., and Akira, S. (2003) *Science* **301,** 640–643
20. Kawai, T., Takahashi, K., Sato, S., Coban, C., Kumar, H., Kato, H., Ishii, K. J., Takeuchi, O., and Akira, S. (2005) *Nat. Immunol.* **6,** 981–988
21. Seth, R. B., Sun, L., Ea, C. K., and Chen, Z. J. (2005) *Cell* **122,** 669–682
22. Meylan, E., Curran, J., Hofmann, K., Moradpour, D., Binder, M., Bartenschlager, R., and Tschopp, J. (2005) *Nature* **437,** 1167–1172
23. Xu, L. G., Wang, Y. Y., Han, K. J., Li, L. Y., Zhai, Z., and Shu, H. B. (2005) *Mol. Cell* **19,** 727–740
24. Lee, H. K., Dunzendorfer, S., Soldau, K., and Tobias, P. S. (2006) *Immunity* **24,** 153–163
25. Limmon, G. V., Arredouani, M., McCann, K. L., Corn Minor, R. A., Kobzik, L., and Imani, F. (2008) *FASEB J.* **22,** 159–167
26. Krieg, A. M. (2002) *Annu. Rev. Immunol.* **20,** 709–760
27. Itoh, K., Watanabe, A., Funami, K., Seya, T., and Matsumoto, M. (2008) *J. Immunol.* **181,** 5522–5529
28. Ranjith-Kumar, C. T., Duffy, K. E., Jordan, J. L., Eaton-Bassiri, A., Vaughan, R., Hoose, S. A., Lamb, R. J., Sarisky, R. T., and Kao, C. C. (2008) *Mol. Cell. Biol.* **28,** 4507–4519
29. Saeki, K., Miura, Y., Aki, D., Kurosaki, T., and Yoshimura, A. (2003) *EMBO J.* **22,** 3015–3026
30. Obuse, C., Iwasaki, O., Kiyomitsu, T., Goshima, G., Toyoda, Y., and Yanagida, M. (2004) *Nat. Cell Biol.* **6,** 1135–1141
31. Ebihara, T., Shingai, M., Matsumoto, M., Wakita, T., and Seya, T. (2008) *Hepatology* **48,** 48–58
32. Ding, C., Wang, L., Al-Ghawi, H., Marroquin, J., Mamula, M., and Yan, J. (2006) *Eur. J. Immunol.* **36,** 2013–2024
33. Saeki, K., Fukuyama, S., Ayada, T., Nakaya, M., Aki, D., Takaesu, G., Hanada, T., Matsumura, Y., Kobayashi, T., Nakagawa, R., and Yoshimura, A. (2009) *J. Immunol.* **182,** 5929–5937
34. Ohno H. (2006) *J. Cell Sci.* **119,** 3719–3721
35. Tian, J., Avalos, A. M., Mao, S. Y., Chen, B., Senthil, K., Wu, H., Parroche, P., Drabic, S., Golenbock, D., Sirois, C., Hua, J., An, L. L., Audoly, L., La Rosa, G., Bierhaus, A., Naworth, P., Marshak-Rothstein, A., Crow, M. K., Fitzgerald, K. A., Latz, E., Kiener, P. A., and Coyle, A. J. (2007) *Nat. Immunol.* **8,** 487–496

ELSEVIER

INSTITUT PASTEUR

Microbes and Infection 13 (2011) 350e358

www.elsevier.com/locate/micinf

Original article

Failure of mycoplasma lipoprotein MALP-2 to induce NK cell activation through dendritic cell TLR2

Ryoko Sawahata [a,1], Hiroaki Shime [a,1], Sayuri Yamazaki [a], Norimitsu Inoue [b], Takashi Akazawa [b], Yukari Fujimoto [c], Koichi Fukase [c], Misako Matsumoto [a], Tsukasa Seya [a,*]

[a] Department of Microbiology and Immunology, Graduate School of Medicine, Hokkaido University, N-15 W-7, Kita-ku, Sapporo 060-8638,Japan
[b] Department of Molecular Genetics, Osaka Medical Center for Cancer, Nakamichi 1-3-2, Higashinari-ku, Osaka 537-8511, Japan
[c] Department of Chemistry, Graduate School of Science, Osaka University, Toyonaka, Osaka 560-0043, Japan

Received 1 September 2010; accepted 9 December 2010
Available online 21 December 2010

Abstract

Macrophage-activating lipopeptide 2 (MALP-2), a mycoplasmal diacylated lipopeptide with palmitic acid moiety (Pam2), activates Toll-like receptor (TLR) 2 to induce inflammatory cytokines. TLR2 is known to mature myeloid dendritic cells (mDC) to drive mDC contact-mediated natural killer (NK) cell activation. Here we tested if MALP-2 activates NK cells through stimulation of TLR2 on mDC. Although synthetic MALP-2 with 6 or 14 amino acids (a.a.) stretch (designated as s and f) matured mDC to induce IL-6, IL-12p40 and TNF-a to a similar extent, they far less activated NK cells than Pam2CSK4, a positive control of 6 a.a.-containing diacyl lipopeptide. MALP-2s and f were TLR2/6 agonists and activate the MyD88 pathway similar to Pam2CSK4, but MALP-2s having the CGNNDE sequence acted on mDC TLR2 to barely induce external NK activation. Even the s form, with slightly high induction of IL-6 compared to the f form, barely induced in vivo growth retardation of NK-sensitive implant tumor. Pam2CSK4 and MALP-2 have the common lipid moiety but different peptides, which are crucial for NK cell activation. The results infer that MALP-2 is applicable to a cytokine inducer but not to an adjuvant for antitumor NK immunotherapy.

Keywords: Toll-like receptor 2; MyD88; Macrophage-activating lipopeptide 2; Dendritic cells; NK activation

1. Introduction

Macrophage-activating lipopeptide 2 (MALP-2) is a mycoplasmal diacylated lipopeptide with agonistic activity for Toll-like receptor (TLR) 2 [1]. Myeloid dendritic cells (mDC) and macrophages produce inflammatory cytokines in response to MALP-2 [1,2]. MALP-2 is proteolytically liberated from the parent lipoprotein of M161Ag [2,3] or MALP-404 [4], which is anchored on the outer membrane of Mycoplasma fermentans. Although the protease that specifically cleaves M161Ag into MALP-2 has not been identified, the peptide sequence of MALP-2 is determined by Mass spectrometry as S-[2,3-bis (palmitoyl)propyl]cysteine (Pam2Cys) followed by 14 amino acids [5] (Table 1). In fact, the TLR2 agonistic functions are conserved in a synthetic compound (herein referred to MALP-2f) [5]. This synthetic MALP-2 has been applied to clinical phase studies to develop a new adjuvant [6].

Several reports suggested that microbial pattern molecules have the ability to activate natural killer (NK) cells in vitro [7 e 10]. TLR and cytoplasmic pattern sensors are representative pattern-recognition receptors (PRR) which may be associated with mDC-mediated NK activation [7 e 9]. TLR3 and the adapter TICAM-1 (TRIF) in mDC typically participate in driving NK activation in response to dsRNA [10]. Recent studies on TLR2 agonists including lipopeptides also revealed that stimulation of TLR2 on mDC results in activation of the MyD88 pathway in mDC to drive external NK activation [11,12]. NK cells play a role in early defense against various pathogens.

* Corresponding author. Tel.: þ81 11 706 5073; fax: þ81 11 706 7866.
E-mail address: seya-tu@pop.med.hokudai.ac.jp (T. Seya).
[1] First two authors equally contributed to this work.

1286-4579/$ - see front matter
doi:10.1016/j.micinf.2010.12.003

Table 1
Lipopeptides used in this study.

Name	Peptide structure	Mr (Dalton)	Ref.
Pam2CSK	CSK	887.3	[19]
Pam2CSK4	CSKKKK	1271.8	[13]
Pam2Cys12	CSTSEVIGEKI	1716.2	[19]
MALP-2s	CGNNDE	1201.5	(*)[a]
MALP-2f	CGNNDESNISFKEK	2135.6	[13]

[a] * e This paper.

We have looked into the immuno-modulatory function of M161Ag and MALP-2, to develop a new adjuvant for cancer immunotherapy [1]. MALP-2 possessed high activity to induce IL-6, TNF-a, IL-10 and IL-12p40 from myeloid cells, but its functional potential for NK activation has not been examined yet. We test in the present studies whether MALP-2 has sufficient activity to induce NK cell activation in vitro and NK-mediated tumor regression in vivo using a mouse tumor implant model.

2. Materials and methods

2.1. Reagents and antibodies

The following materials were obtained as indicated: Fetal calf serum (FCS) from Bio Whittaker (Walkersville, MD), mouse granulocyte-macrophage colony-stimulating factor (GM-CSF) from PeproTech EC, Ltd (London, UK), the enzyme-linked immunosorbent assay (ELISA) kits for mouse (m)IFN-g from Biolegend (San Diego, CA), IL-12p40, IL-12p70, and IL-6 from eBioscience (San Diego, CA). Two forms of synthetic macrophage-activating lipopeptide 2 (MALP-2) were ordered to Biologica Co., Nagoya, Japan. MALP-2s: Pam2CGNNDE (MW; 1201.5) and MALP-2f: Pam2CGNNDESNISFKEK (MW; 2135.6). The synthesis of lipopeptides was achieved with a combination of solution- and solid-phase methods as described [13]. Pam2Cys12 (Pam_2CSTSEVIGEKI), Pam2CSK4 (Pam_2CSKKKK) and control Pam2CSK were prepared as referenced [12]. PolyI:C, a TLR3 agonist for induction of anti-tumor immunity, was used for this study as a positive control.

The following antibodies were used: fluorescein isothiocyanate (FITC)-labeled anti-mouse CD69, I-Ab, IFN-a mAb, phycoerythrin (PE)-labeled anti-mouse CD86, CD25, and allophycocyanin (APC)-labeled anti-mouse NK1.1 were purchased from Biolegend (San Diego, CA).

2.2. Mouse and cell lines

TLR2 / and MyD88 / mice were gifts from Dr. S. Akira (Osaka Univ., Osaka) as previously reported [14]. Female C57BL/6 mice were purchased from Clea Japan (Tokyo). Mice were maintained in our institute under specific pathogen-free conditions. All animal work was performed under guidelines established by the Hokkaido University Animal Care and Use Committee. Mice (12 weeks female C57BL/6) were housed four per cage and allowed food and water ad libitum. Animal studies were carefully performed without ethical problems.

HEK293 cells were obtained from ATCC and maintained in RPMI 1640/10% FCS. B16D8 cells were established in our laboratory as a subline of the B16 melanoma cell line [15] and cultured in RPMI 1640/10% FCS. This subline was characterized by its low MHC levels with no metastatic properties when injected s.c. into syngeneic C57BL/6 mice. The B16D8 cell line is a typical NK target [10].

2.3. Preparation of BMDC and spleen NK cells of mice

Mouse bone marrow-derived DC (BMDC) were prepared as described previously [16]. Spleen NK cells were positively isolated from spleens with DX5 Micro Beads kit (Miltenyi Biotech) [10]. The purity of NK cells ($DX5^b$ cells) was routinely about 80%. $DX5^b$ NK cells were used within 24 h.

2.4. Reporter assay

Plasmids (pEFBos) for expression of human TLR1, TLR2, TLR6 and TLR10 were prepared in our laboratory as described previously [16]. HEK293 cells were seeded onto 24-well plates and transfected with various amounts of expression vectors, the ELAM reporter gene, and the phRL-TK control plasmid using FuGene HD (Roche) according to the manufacturer's instructions. After 24 h, the cells were harvested in 50 ml lysis buffer. The luciferase activity was measured using Dual-Luciferase Reporter assay systems (Promega) and was shown as the mean S.D. of three experiments.

2.5. ELISA, flow cytometric (FACS) analysis of cell surface antigens

The levels of cytokines (IL-6, IL-12p40, IFN-g etc.) were determined by sandwich ELISA (Amersham Pharmacia Biotech, Buckinghamshire, UK) or the message levels assessed by quantitative PCR [27]. Surface CD86 and I-Ab were determined by FACS using specific mAbs. The practical methods for FACS were described previously [16].

2.6. Assessment of in vitro cytolytic activity

The cytolytic activity of spleen NK cells was determined by ^{51}Cr assay as described previously [10]. NK cells were prepared from the spleen of C57BL/6 mice. NK cells were co-cultured with BMDCs at a ratio of 2:1 and 24 h later the mixtures were subdivided to assess NK-mediated cytotoxicity [10]. A B16 subline (D8) was used as a target cell. Target cells (2 10^3 cells/well) were coincubated with NK cells at the indicated lymphocyte to target (E/T) cell ratio (typically 20) in U-bottom 96-well plates in a total volume of 200 ml of RPMI 1640/10% FCS medium at 37 C. Four hours later, the liberated ^{51}Cr in the medium was measured using the scintillation counter. Specific cytolytic activity was obtained by the formula: Specific cytotoxic activity (%) ¼ [(experimental ^{51}Cr activity spontaneous ^{51}Cr activity)/(total ^{51}Cr activity spontaneous ^{51}Cr activity)] 100. Each experiment was done in triplicate to confirm reproducibility of the results, and representative results are shown.

2.7. Tumor challenge and the treatment with Pam2Cys-containing peptides

B16D8 cells (6 10^5 cells) were subcutaneously (s.c.) transplanted into the back of mice at day 0. Pam2Cys-containing peptides (10 mg/head) or PBS (vehicle) only were injected around tumor at day 0, 3, 7, 9, 13, and 17. Tumor surfaces were measured twice a week by using a caliper.

3. Results

3.1. BMDC maturation and cytokine liberation in response to MALP-2

Pam2Cys-containing lipopeptides, Pam2Cys12, Pam2CSK, Pam2CSK4, and two forms of MALP-2 (s and f) were synthesized with reference to a previous report (Table 1) [13,17]. Pam2CSK was used as a negative control [17], which has virtually no cytokine-inducing activity (Fig. 1). By ELAM reporter assay, we assessed NF-kB activation potential of these lipopeptides (10e500 nM), and confirmed that all except Pam2CSK possess similar luciferin-activating potentials (data not shown).

IL-6 and IL-12p40 levels were determined by ELISA with the supernatant of the media where BMDC and each of the lipopeptides were co-cultured for 24 h. These cytokines were detected with high levels in the wells with Pam2Cys12, Pam2CSK4, MALP-2s and MALP-2f but not in Pam2CSK (Fig. 1A,B). These lipopeptides neither induced the mRNA of type I interferon (IFN), IL-15 and IL-8 (data not shown) or produced less than the detection limit (<5 pg/ml) of IL-12p70 protein (Fig. 1C).

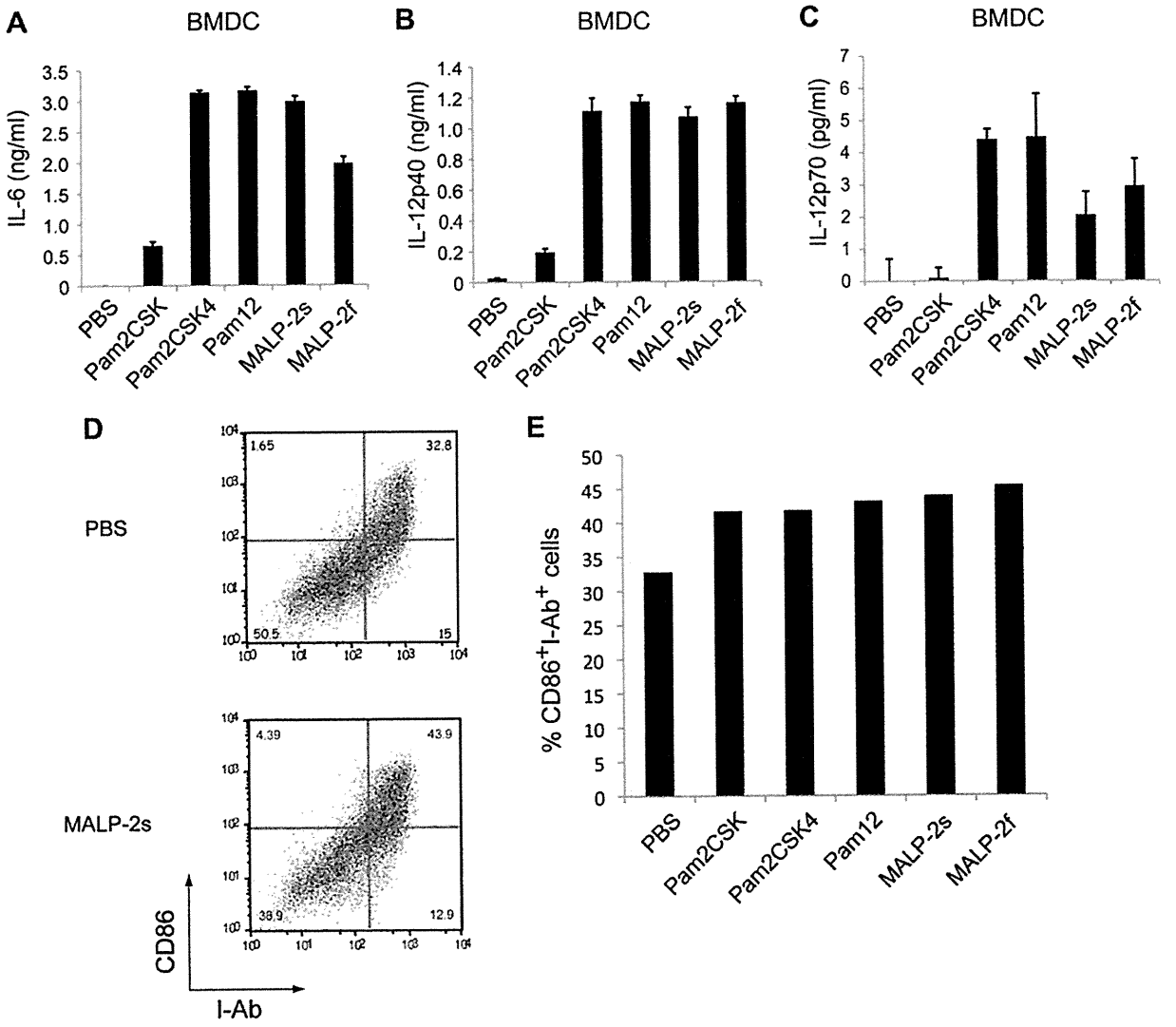

Fig. 1. BMDC cytokine production and maturation in response to TLR2 agonists (A, B, C) Cytokine production by BMDC stimulated with Pam2Cys-containing peptides. BMDC prepared from wild-type mice were treated with indicated Pam2Cys-containing peptides (100 nM) for 24 h. IL-6 (A), IL-12p40 (B), and IL-12p70 (C) concentrations in the supernatant were measured by ELISA. (D, E) Flow cytometric analysis of CD86 and I-Ab expression of BMDC stimulated with Pam2Cys-containing peptides. Typical examples of flow cytometric analysis (D). Summary of CD86 and I-Ab expression on the BMDC (E).

The degrees of CD86 up-regulation were examined with these lipopeptides, and similar DC maturation was evaluated by flow cytometry (Fig. 1D,E). Although the levels of CD86 were increased in response to Pam2 peptides (100 nM), no significant difference was observed among the Pam2 peptides tested (Fig. 1E). At the dose of Pam2 where cytokine induction sufficiently occurs, CD86 expression inadequately takes place in BMDC, as reported previously [12]. Thus, NF-kB activation, cytokine liberation and DC maturation are partially co-related in these lipopeptides.

3.2. NK activation by Pam2CSK4 and MALP-2

Previous reports suggested that TLR2 agonists have ability to induce NK activation [11,12]. To investigate whether the Mycoplasma lipopeptides harbor activity of NK cell activation, we added the Pam2Cys peptides (100 nM) to BMDC, NK cells or BMDC/NK co-culture as in a previous method assessing polyI:C activity for BMDC-mediated NK activation [10]. Although BMDC per se can induce IFN-g production in response to some TLR stimuli [17,18], we could detect only minute amounts of IFN-g in our setting using Pam2 lipopeptides (Fig. 2A). In this context, three markers for NK activation [19] were assessed with this system, IFN-g production, up-regulation of NK activation markers and target cell (B16D8) cytotoxicity by NK cells (Fig. 2). IFN-g was generated in the supernatants (sup) of NK cells (Fig. 2B) or BMDC/NK co-culture (Figs. 2C and 3A left hand panel) in response to the control lipopeptides, Pam2CSK4 and Pam2-Cys12. However, MALP-2s and f showed significantly low potentials for IFN-g-induction comparable to the negative control Pam2CSK.

The NK cell activation markers CD25 and CD69 were analyzed with BMDC co-cultured NK cells with or without the lipopeptide treatment by flow cytometry (Fig. 2D). Up-regulation of surface CD25 and CD69 was observed in NK cells incubated with BMDC stimulated with Pam2CSK4 and Pam2Cys12 but far less with MALP-2s and f.

Activated NK cells are a major source of IFN-g which causes a variety of responses of the immune system. To further examine whether BMDC matured with Pam2CSK4 or MALP-2 drive NK-dependent IFN-g secretion, we stimulated BMDC with these lipopeptide reagents for 4 h and then mixed with NK cells (ratio 1:2) for 20 h. Breferdin was added to the mixture in order to accumulate IFN-g in the NK cells for the last 4 h of incubation. As shown in Fig. 2E, the TLR2 ligands Pam2CSK4 and Pam2Cys12 significantly increased the frequency of IFN-g-secreting NK cells, while MALP-2f and s showed far less activity to produce IFN-g in the NK cells.

Cytotoxic activity was evaluated using B16D8 cells as a target [10]. BMDC-activated NK cells (see above) were incubated with B16D8 cells at a ratio of 30:1. Again, MALP-2s and f showed less effective killing against the target (Fig. 3B left hand panel). The other lipopeptides had sufficient killing activity compared to the control polyI:C: one of two examples assayed with different BMDC lots are shown in the figure.

3.3. Participation of TLR2/MyD88 in MALP-2-mediated NK activation

We next examined whether the lipopeptide-mediated IFN-g secretion was dependent on MyD88 of BMDC. IFN-g secretion was almost completely abrogated in the co-culture with MyD88 / BMDC and wild-type NK cells in the presence of Pam2Cys12 and Pam2CSK4 (Fig. 3A), Similar tendencies were observed with MALP-2 peptides, which essentially evoked a minimal IFN-g production, and the IFN-g-induction was largely abrogated with MyD88 / BMDC (Fig. 3A). The results were less prominently reproduced with TLR2 / BMDC and wild-type NK cells (data not shown). Further confirmation was performed using the mixtures with wild-type NK cells and various lipopeptides. No direct activation of NK cells was observed in the absence of BMDC (data not shown).

The results were further confirmed with NK cytotoxic assay using NK cells co-cultured with Pam2Cys lipopeptide-stimulated BMDC (Fig. 3B). When wild-type BMDC was used as an NK cell cytotoxicity inducer, full NK activation was induced by Pam2Cys12 or Pam2CSK4. MALP-2f and s were found to be inefficient NK activators (Fig. 3B). If wild-type BMDC were replaced with MyD88 / BMDC, BMDC-enhanced NK cytotoxicity was abrogated (Fig. 3B). The MyD88 pathway in BMDC is crucial for BMDC-mediated NK cell activation.

3.4. Combinational recognition of MALP-2s and f by TLR2 and TLR6

TLR2 recognizes diacyl lipopeptide in combination with TLR6 [20] while TLR2 recognizes triacyl lipopeptide together with TLR1 [21]. We found TLR2/6 cooperate to recognize Staphylococcus aureus lipopeptides using HEK293 cells with TLR2/6 expression. Data testing MALP-2f for the usage of TLR2/6 are shown in Fig. 4. Single receptors of TLR1, TLR6 and TLR10 barely activate NF-kB by reporter assay and only TLR2 exhibited <60 fold ELAM promoter activation (data not shown). No enhanced activation was observed in combination with TLR2 and TLR1 or TLR2 and TLR10. Similar results on TLR2/6-mediated augmentation of reporter activation were observed with MALP-2s and Pam2CSK4 (data not shown). Hence, TLR6 helps to amplify the TLR2 signal by MALP-2 lipopeptide as in other Pam2Cys lipopeptides, but IFN-g was minimally induced in the NK cells.

3.5. Antitumor adjuvant activity against NK-sensitive tumor in vivo

Recent studies revealed that intratumoral or i.p. injection of MALP-2 supresses pancreatic carcinoma in a mouse model [22]. Tumor suppression is also observed with Pam2Cys type lipopeptides in B16D8 (NK-sensitive) implant mice [23]. The antitumor function by MALP-2 is abrogated in MyD88 / mice, suggesting that TLR2/MyD88 and following cell-mediated immunity play a major part of tumor suppression [23]. We tested whether MALP-2 injected s.c. induces growth

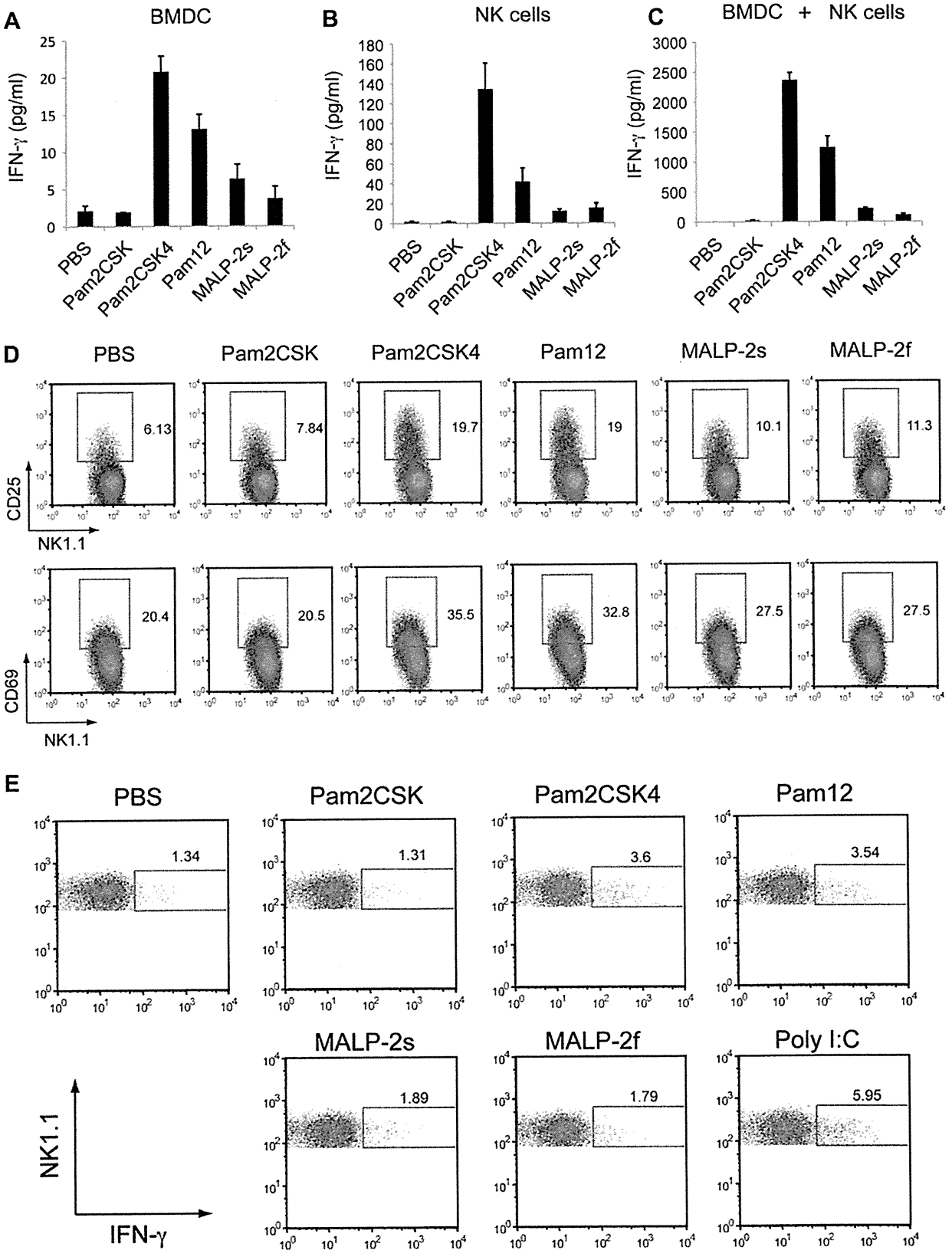
A
BMDC
IFN-γ (pg/ml)
PBS
Pam2CSK
Pam2CSK4
Pam12
MALP-2s
MALP-2f
B
NK cells
C
BMDC + NK cells
D
CD25
NK1.1
CD69
6.13
7.84
19.7
19
10.1
11.3
20.4
20.5
35.5
32.8
27.5
27.5
E
1.34
1.31
3.6
3.54
1.89
1.79
5.95
Poly I:C
IFN-γ

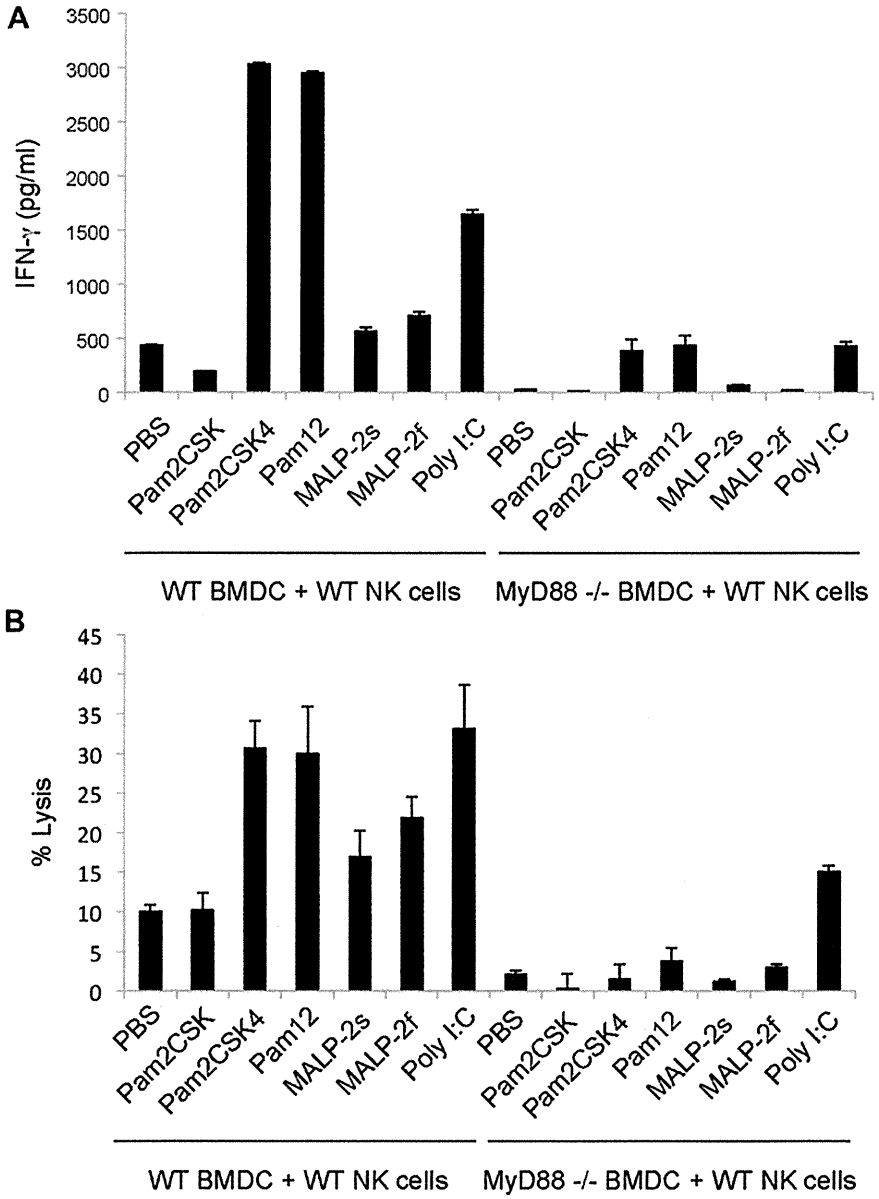

Fig. 3. IFN-g production and cytotoxic activity of NK cells co-cultured with BMDC in the presence of Pam2Cys-containing peptides. Wild-type and MyD88 / BMDC were stimulated with Pam2Cys-containing peptides for 4 h. Then, the BMDC were co-cultured with wild-type NK cells for 24 h (A) IFN-g levels in culture supernatant were determined by ELISA. (B) Cytotoxic activities of NK cells were measured by ^{51}Cr release assay. B16D8 cells were used as a target. E/T ratio ¼ 20.

retardation of the tumor (NK target B16D8 cells) via NK activation (Fig. 5). Pam2CSK4 s.c. injected around tumor exhibited tumor growth retardation (Fig. 5A). This Pam2CSK4 activity was abrogated by injection of asialoGM-1 Ab (data not shown). In contrast, no tumor growth retardation was observed in this NK-sensitive tumor by s.c. injected MALP-2 (Fig. 5B). The results infer that MALP-2 exerts only minimal potential if any, to activate NK cells through BMDC in vitro and vivo. Unlike BCG-CWS [19] or polyI:C [8 e 10], MALP-2 barely suppresses tumor growth in this mouse system.

Fig. 2. Pam2Cys-containing peptides activate NK cells through TLR2 in BMDC. (A, B, C) BMDC and NK cells prepared from wild-type mice were stimulated with Pam2Cys-containing peptides for 24 h (A, B). Alternatively, BMDC were stimulated with Pam2Cys-containing peptides for 4 h. Then, NK cells prepared from wild-type mouse spleen were co-cultured with the BMDC for 24 h. IFN-g levels in the culture supernatant are shown. (D) CD25 and CD69 expression on NK cells co-cultured with BMDC in the presence of Pam2Cys-containing peptides. The NK cell populations (marked with NK1.1) were gated on the display of FACS and levels of CD25 or CD69 (inset values) were examined as shown in the graphs. (E) Intracellular IFN-g staining of NK cells co-cultured with BMDC in the presence of Pam2Cys-containing peptides as above. Cells were treated with breferdin and then permeabilized. Intracellular IFN-g was detected by specific mAb. IFN-g positive cells are marked with square and their frequencies are indicated by inset values.

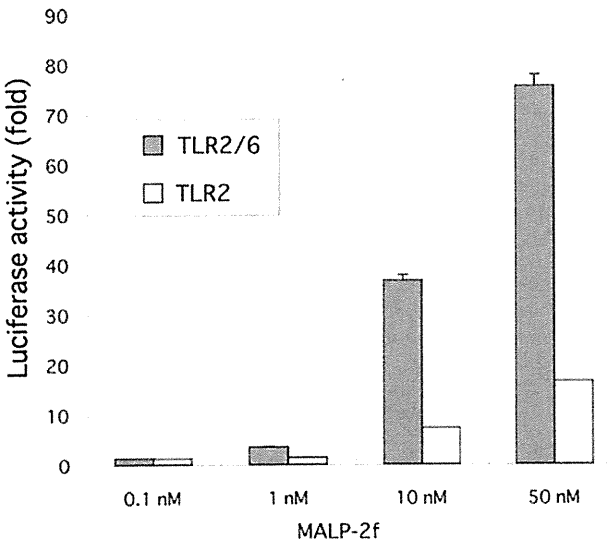

Fig. 4. TLR6 facilitates the recognition of MALP-2 by TLR2. HEK293 cells were transfected with the plasmids encoding TLR2 and/or TLR6, and ELAM-luciferase reporter. After 24 h, the cells were treated with MALP-2f for 6 h. Then, luciferase activity of the cell lysates was measured. Similar results were obtained with MALP-2s (not shown).

4. Discussion

Recent studies demonstrated that mDC induce NK activation by stimulation with TLR2 in mDC [12]. This NK activation occurs in a distinct mode of those reported in the TICAM-1/IPS-1 pathways for type I IFN induction because this NK activation is derived through the MyD88 pathway. Indeed, MyD88 has been reported to participate in NK cell activation induced by Plasmodium falciparum-infected erythrocytes, but TLR2 response was not mandatory in the reported human case [24]. In another report, direct TLR2 stimulation in NK cells but not mDC was critical for NK cell activation in a vaccinia infection system [25]. We then tested whether a TLR2 agonist MALP-2 harbors adjuvant potential of mDC-mediated NK activation in mouse.

NK activation fails to be induced by MALP-2-stimulated mDC judged by IFN-g production, up-regulation of NK activation marker CD25 and CD69, and cytotoxicity against the NK target B16D8 cells. Cytokines with NK activation properties such as IFN-a/b, IL-15 and IL-12p70 are not up-regulated in mDC in response to MALP-2, although a regulatory cytokine IL-10 is produced by stimulation with MALP-2 [3,5]. Finally, s.c. administration of MALP-2 did not result in retardation of tumor growth in mice with B16D8 tumor burden. Although Pam2CSK4 having 6 a.a.-stretch following the diacyl residue acts as an NK-activating reagent [10,18], two forms of MALP-2 with short (6 a.a.) or long (14 a.a.) peptide barely exhibits antitumor activity. Hence, NK activation is a phenotype induced by a limited group of Pam2Cys lipopeptides, and the peptide sequence is critical for inducing mDC-mediated NK activation. Our results infer that TLR2-dependent mDC response to drive NK activation largely relies on the peptide sequences of

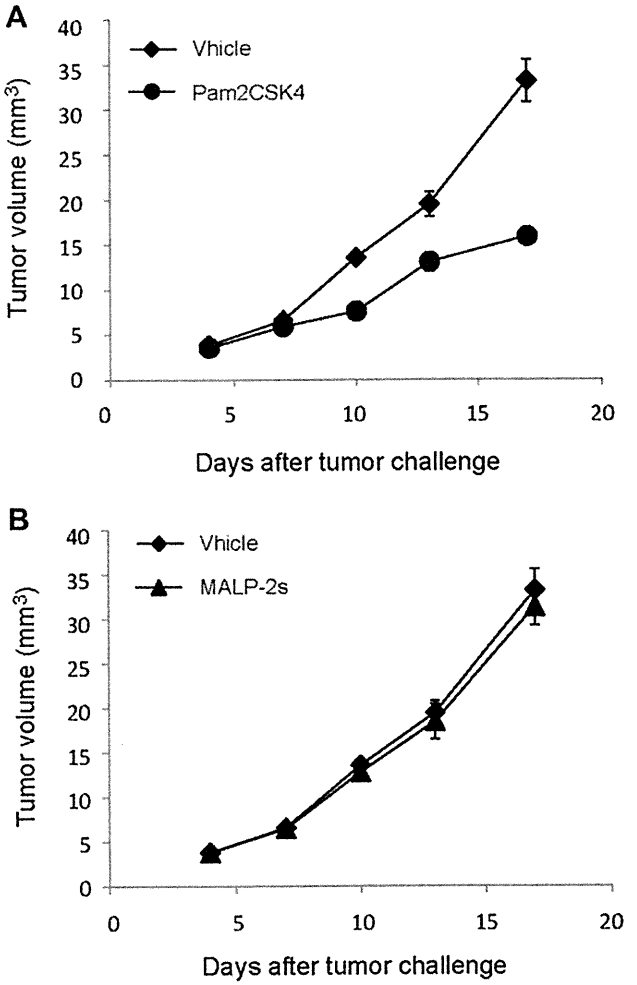

Fig. 5. MALP-2 fails to inhibit tumor growth in vivo. B16D8 cells were transplanted subcutaneously into mice at day 0. Mice (16 week-old, female) were treated with Pam2CSK4 (A) or MALP-2s (B) at day 0, 3, 7, 9, 13, 17 as described in Materials and methods. No tumor growth retardation was observed when MALP-2s was replaced with MALP-2f (not shown). Each group consists of n ¼ 4. Surface diameters of the implanted tumors were measured. Mean SD are shown.

lipoproteins. TLR2-stimulating lipopeptides are not unifunctional: some are active on NK cells but not others.

TLR2 in conjunction with TLR6 serves as an adjuvant receptor with potent cytokine-inducing ability, accompanied with up-regulation of IL-1b, IL-6, IL-12p40 and TNF-a. Apoptosis and NO production are also evoked through TLR2 stimulation [2]. The cytokine profile induced by MALP-2 indicates that macrophages and mDC differentiated from monocytes are targets for MALP-2 via their TLR2. TLR2 agonists facilitate induction of CTL and CD4 T cells against specific antigens [23,26]. In fact, M161Ag potently induces complement-associated inflammation [27] and maturation of immature mDC [16,28]. Although cytoplasmic sensors for bacterial lipoproteins may in part participate in the functional properties of MALP-2 [29], TLR2 agonistic activity in MALP-2 would involve cytokine-inducing properties but not anti-tumor function by intensifying in vivo NK activation.

Adjuvants are important for induction of vaccine immunity. Cancer immunotherapy has been developed using a variety of adjuvants. Intratumoral or intraperitoneal injection of MALP-2 has been attempted to induce suppression of pancreatic carcinoma in a mouse model [22]. In clinical trials, MALP-2 alone or in combination with gemcitabine was used for the treatment of unresectable pancreas carcinoma [6]. The rationale of this approach is based on the ability of MALP-2 to (1) act as a cytokine inducer [30], (2) activate murine as well as human DC to express co-stimulatory molecules [31], (3) induce a T-helper (Th) 1/2 response [32] and, most importantly, prolong survival in a mouse model of an orthotopic, syngeneic pancreas tumor [22]. Although Pam2 lipoproteins often induce an inhibitory cytokine IL-10 and regulatory T cells (Yamazaki S, unpublished data), no report mentioned the effect of these factors on MALP-2 adjuvant potential. We favored interpretation that the beneficial effects were due to immune activation, as we observed an increase in the expression of co-stimulatory molecules on lymphocytes, and cytotoxic T and NK cells infiltrating the tumor. However, our experiments with tumor-loaded mice showed that s.c. administration of MALP-2 confers no NK cell-mediated tumor regression on B16D8-implant mice. This unexpected result may be due to specific TLR2 agonistic properties of MALP-2 compared to peptidoglycan (that induces IL-12p70 in human mDC) [33] or instability of the lipid moiety of MALP-2. MALP-2 is degraded by two different mechanism in inflamed tissue: de-esterification and oxidation of the thioester bridge [6,34], thereby disappearing from the skin with a half time of w 20 h. Further modification will be required for in vivo use of this reagent.

Acknowledgments

We thank Drs. J. Kasamatsu, H. Takaki, A. H. Hussein, A. Watanabe and H. Oshiumi in our laboratory for their critical discussions. This work was supported in part by Grants-in-Aid from the Ministry of Education, Science, and Culture (Specified Project for Advanced Research) and the Ministry of Health, Labor, and Welfare of Japan, and by the Yakult and Waxmann Foundations. Financial supports by the Sapporo Biocluster "Bio-S" the Knowledge Cluster Initiative of the MEXT, is gratefully acknowledged.

References

[1] T. Seya, M. Matsumoto, A lipoprotein family from Mycoplasma fermentans confers host immune activation through Toll-like receptor 2, Int. J. Biochem. Cell Biol. 34 (2002) 901e906.

[2] M. Matsumoto, M. Nishiguchi, S. Kikkawa, H. Nishimura, S. Nagasawa, T. Seya, Structural and functional properties of complement-activating protein M161Ag, a Mycoplasma fermentans gene product that induces cytokine production by human monocytes, J. Biol. Chem. 273 (1998) 12407e12414.

[3] M. Matsumoto, J. Takeda, N. Inoue, T. Hara, M. Hatanaka, K. Takahashi, S. Nagasawa, H. Akedo, T. Seya, A novel protein that participates in non-self discrimination of malignant cells by homologous complement, Nat. Med. 3 (1997) 1266e1270.

[4] K.L. Davis, K.S. Wise, Site-specific proteolysis of the MALP-404 lipoprotein determines the release of a soluble selective lipoprotein-associated motif-containing fragment and alteration of the surface phenotype of Mycoplasma fermentans, Infect. Immun. 70 (2002) 1129e1135.

[5] P.F. Mühlradt, M. Kiess, H. Meyer, R. Süssmuth, G. Jung, Isolation, structure elucidation, and synthesis of a macrophage stimulatory lipopeptide from Mycoplasma fermentans acting at picomolar concentration, J. Exp. Med. 185 (1997) 1951e1958.

[6] J. Schmidt, T. Welsch, D. Jäger, P.F. Mühlradt, M.W. Büchler, A. Märten, Intratumoral injection of the Toll-like receptor-2/6 agonist 'macrophage-activating lipopeptide-2' in patients with pancreatic carcinoma: a phase I/II trial, Br. J. Cancer 97 (2007) 598e604.

[7] D. Haller, P. Serrant, D. Granato, E.J. Schiffrin, S. Blum, Activation of human NK cells by staphylococci and lactobacilli requires cell contact-dependent costimulation by autologous monocytes, Clin. Diagn. Lab. Immunol. 9 (2002) 649e657.

[8] T. Miyake, Y. Kumagai, H. Kato, Z. Guo, K. Matsushita, T. Satoh, T. Kawagoe, H. Kumar, M.H. Jang, T. Kawai, T. Tani, O. Takeuchi, S. Akira, Poly I: C-induced activation of NK cells by CD8 alpha þ dendritic cells via the IPS-1 and TRIF-dependent pathways, J. Immunol. 183 (2009) 2522e2528.

[9] S. McCartney, W. Vermi, S. Gilfillan, M. Cella, T.L. Murphy, R.D. Schreiber, K.M. Murphy, M. Colonna, Distinct and complementary functions of MDA5 and TLR3 in poly(I:C)-mediated activation of mouse NK cells, J. Exp. Med. 206 (2009) 2967e2976.

[10] T. Akazawa, M. Okuno, Y. Okuda, K. Tsujimura, T. Takahashi, M. Ikawa, M. Okabe, T. Ebihara, M. Shingai, N. Inoue, M. Tanaka-Okamoto, H. Ishizaki, J. Miyoshi, M. Matsumoto, T. Seya, Antitumor NK activation induced by the Toll-like receptor3-TICAM-1 (TRIF) pathway in myeloid dendritic cells, Proc. Natl. Acad. Sci. U S A 104 (2007) 252e257.

[11] Y. Akao, T. Ebihara, H. Masuda, Y. Saeki, K. Hazeki, O. Hazeki, M. Matsumoto, T. Seya, Enhancement of antitumor natural killer cell activation by orally administered Spirulina extract in mice, Cancer Sci. 100 (2009) 1494e1501.

[12] M. Azuma, R. Sawahata, Y. Akao, T. Ebihara, S. Yamazaki, M. Matsumoto, M. Hashimoto, K. Fukase, Y. Fujimoto, T. Seya, The peptide sequence of diacyl lipopeptides determines dendritic cell TLR2-mediated NK activation, PLoS One 5 (2010) e12550.

[13] Y. Fujimoto, M. Hashimoto, M. Furuyashiki, M. Katsumoto, T. Seya, Y. Suda, K. Fukase, Innate immunostimulatory lipopeptides of Staphylococcus aureus as TLR2 ligands; Prediction with mRNA expression, chemical synthesis and immunostimulatory activities, Chembiochem 10 (2009) 2311e2315.

[14] O. Takeuchi, K. Hoshino, T. Kawai, H. Sanjo, H. Takada, T. Ogawa, K. Takeda, S. Akira, Differential roles of TLR2 and TLR4 in recognition of gram-negative and gram-positive bacterial cell wall components, Immunity 11 (1999) 443e451.

[15] H. Tanaka, Y. Mori, H. Ishii, H. Akedo, Enhancement of metastatic capacity of fibroblast-tumor cell interaction in mice, Cancer Res. 48 (1988) 1456e1459.

[16] M. Nishiguchi, M. Matsumoto, T. Takao, M. Hoshino, Y. Shimonishi, S. Tsuji, O. Takeuchi, S. Akira, K. Toyoshima, T. Seya, Mycoplasma fermentans lipoprotein M161Ag-induced cell activation is mediated by Toll-like receptor 2: role of N-terminal hydrophobic portion in its multiple functions, J. Immunol. 166 (2001) 2610e2616.

[17] D.M. Frucht, T. Fukao, C. Bogdan, H. Schindler, J.J. O'Shea, S. Koyasu, IFN-gamma production by antigen-presenting cells: mechanisms emerge, Trends Immunol. 22 (2001) 556e560.

[18] I. Fricke, D. Mitchell, J. Mittelstädt, N. Lehan, H. Heine, T. Goldmann, A. Böhle, S. Brandau, Mycobacteria induce IFN-gamma production in human dendritic cells via triggering of TLR2, J. Immunol. 176 (2006) 5173e5182.

[19] T. Akazawa, N. Inoue, H. Shime, K. Sugiura, K. Kodama, M. Matsumoto, T. Seya, Adjuvant engineering for cancer immunotherapy: development of a synthetic TLR2 ligand with increased cell adhesion, Cancer Sci. 101 (2010) 1596e1603.

[20] O. Takeuchi, T. Kawai, P.F. Mühlradt, M. Morr, J.D. Radolf, A. Zychlinsky, K. Takeda, S. Akira, Discrimination of bacterial lipoproteins by Toll-like receptor 6, Int. Immunol. 13 (2001) 933e940.

[21] O. Takeuchi, S. Sato, T. Horiuchi, K. Hoshino, K. Takeda, Z. Dong, R.L. Modlin, S. Akira, Cutting edge: role of Toll-like receptor 1 in mediating immune response to microbial lipoproteins, J. Immunol. 169 (2002) 10e14.

[22] C. Schneider, T. Schmidt, C. Ziske, K. Tiemann, K. Lee, V. Uhlinsky, P. Behrens, T. Sauerbruch, I. Schmidt-Wolf, P. Mühlradt, J. Schmidt, A. Märten, Tumoursuppression induced by macrophage activating lipopeptide in an ultrasound-guided syngeneic pancreatic carcinoma mouse model, Gut 53 (2003) 355e363.

[23] T. Akazawa, H. Masuda, Y. Saeki, M. Matsumoto, K. Takeda, S. Akira, K. Tsujimura, K. Kuzushima, T. Takahashi, I. Azuma, S. Akira, K. Toyoshima, T. Seya, Adjuvant-mediated tumor regression and tumor-specific cytotoxic response are impaired in MyD88-deficient mice, Cancer Res. 64 (2004) 757e764.

[24] M. Baratin, S. Roetynck, C. Lépolard, C. Falk, S. Sawadogo, S. Uematsu, S. Akira, B. Ryffel, J.G. Tiraby, L. Alexopoulou, C.J. Kirschning, J. Gysin, E. Vivier, S. Ugolini, Natural killer cell and macrophage cooperation in MyD88-dependent innate responses to Plasmodium falciparum, Proc. Natl. Acad. Sci. U S A 102 (2005) 14747e14752.

[25] J. Martinez, X. Huang, Y. Yang, Direct TLR2 signaling is critical for NK cell activation and function in response to vaccinia viral infection, PLoS Pathog. 6 (2010) e1000811.

[26] M.H. Wenink, K.C.M. Santegoets, J.C.A. Broen, L. van Bon, S. Abdollahi-Roodsaz, C. Popa, R. Huijbens, T. Remijn, E. Lubberts, P.L.C. M. van Riel, W.B. van den Berg, TR.D.J. Radstake, TLR2 promotes Th2/Th17 responses via TLR4 and TLR7/8 by abrogating the type I IFN amplification loop, J. Immunol. 183 (2009) 6960e6970.

[27] S. Kikkawa, M. Matsumoto, T. Sasaki, M. Nishiguchi, K. Tanaka, K. Toyoshima, T. Seya, Complement activation on Mycoplasma fermentans induced mycoplasma clearance from infected cells: Probing the organism with mAbs against M161Ag, Infect. Immun. 68 (2000) 1672e1680.

[28] Y. Nakao, K. Funami, S. Kikkawa, M. Taniguchi, M. Nishiguchi, Y. Fukumori, T. Seya, M. Matsumoto, Surface-expressed TLR6 participates in the recognition of diacylated lipopeptide and peptidoglycan in human cells, J. Immunol. 174 (2005) 1566e1573.

[29] U. Buwitt-Beckmann, H. Heine, K.H. Wiesmüller, G. Jung, R. Brock, S. Akira, A.J. Ulmer, TLR1- and TLR6-independent recognition of bacterial lipopeptides, J. Biol. Chem. 281 (2006) 9049e9057.

[30] F. Rharbaoui, B. Drabner, S. Borsutzky, U. Winckler, M. Morr, B. Ensoli, P.F. Muhlradt, C.A. Guzman, The mycoplasma-derived lipopeptide MALP-2 is a potent mucosal adjuvant, Eur. J. Immunol. 32 (2002) 2857e2865.

[31] H. Weigt, P. Mühlradt, A. Emmendörfer, N. Krug, A. Braun, Synthetic derived mycoplasmal lipopeptide MALP-2 induces maturation and function of dendritic cells, Immunobiology 207 (2003) 1e11.

[32] F. Wittke, R. Hoffmann, J. Buer, I. Dallmann, K. Oevermann, S. Sel, T. Wandert, A. Ganser, J. Atzpodien, Interleukin 10 (IL-10): an immunosuppressive factor and independent predictor in patients with metastatic renal cell carcinoma, Br. J. Cancer 79 (1999) 1182e1184.

[33] S. Tsuji, M. Matsumoto, O. Takeuchi, S. Akira, I. Azuma, A. Hayashi, K. Toyoshima, T. Seya, Maturation of human dendritic cells by cell-wall skeleton of Mycobacterium bovis Bacillus Calmette-Guerin: involvement of Toll-like receptors, Infect. Immun. 68 (2000) 6883e6890.

[34] P.F. Mühlradt, M. Kiess, H. Meyer, R. Süssmuth, G. Jung, Structure and specific activity of macrophage-stimulating lipopeptides from Mycoplasma hyorhinis, Infect. Immun. 66 (1998) 4804e4810.

MOLECULAR AND CELLULAR BIOLOGY, Sept. 2011, p. 3802–3819 Vol. 31, No. 18
0270-7306/11/$12.00 doi:10.1128/MCB.01368-10

DDX60, a DEXD/H Box Helicase, Is a Novel Antiviral Factor Promoting RIG-I-Like Receptor-Mediated Signaling▽†

Moeko Miyashita,[1,2] Hiroyuki Oshiumi,[1]* Misako Matsumoto,[1] and Tsukasa Seya[1]

Department of Microbiology and Immunology, Graduate School of Medicine,[1] and Graduate School of Life Science,[2] Hokkaido University, Kita-15, Nishi-7, Kita-ku, Sapporo 060-8638, Japan

Received 30 November 2010/Returned for modification 27 December 2010/Accepted 12 July 2011

The cytoplasmic viral RNA sensors RIG-I and MDA5 are important for the production of type I interferon and other inflammatory cytokines. DDX60 is an uncharacterized DEXD/H box RNA helicase similar to *Saccharomyces cerevisiae* Ski2, a cofactor of RNA exosome, which is a protein complex required for the integrity of cytoplasmic RNA. Expression of DDX60 increases after viral infection, and the protein localizes at the cytoplasmic region. After viral infection, the DDX60 protein binds to endogenous RIG-I protein. The protein also binds to MDA5 and LGP2 but not to the downstream factors IPS-1 and IκB kinase ε (IKK-ε). Knockdown analysis shows that DDX60 is required for RIG-I- or MDA5-dependent type I interferon and interferon-inducible gene expression in response to viral infection. However, DDX60 is dispensable for TLR3-mediated signaling. Purified DDX60 helicase domains possess the activity to bind to viral RNA and DNA. Expression of DDX60 promotes the binding of RIG-I to double-stranded RNA. Taken together, our analyses indicate that DDX60 is a novel antiviral helicase promoting RIG-I-like receptor-mediated signaling.

RIG-I and MDA5 are cytoplasmic viral RNA sensors belonging to the group of RIG-I-like receptors (RLRs), which includes LGP2 (57–59). RIG-I recognizes RNAs from vesicular stomatitis virus (VSV), hepatitis C virus (HCV), Sendai virus (SeV), and influenza A virus (21, 36, 37), while MDA5 recognizes RNA from picornaviruses such as encephalomyocarditis virus and poliovirus (PV) (3, 19, 21). RLRs are also involved in the recognition of cytoplasmic B-DNA. RNA polymerase III transcribes cytoplasmic AT-rich double-stranded DNA (dsDNA), and the transcribed RNA is recognized by RIG-I (1, 6). In contrast, Choi et al. have reported that RIG-I associates with dsDNA (7).

When RIG-I or MDA5 is activated by viral infection, the N-terminal caspase recruitment domains (CARDs) associate with the adaptor protein IPS-1 (also called MAVS/Cardif/VISA) on the outer mitochondrial membrane (22, 26, 42, 55). After this association occurs, IPS-1 activates TBK1 and IκB kinase ε (IKK-ε) and signals interferon (IFN) regulatory factor 3 (IRF-3)- and NF-κB-responsive genes, such as those for type I IFNs or other inflammatory cytokines (22, 23, 26, 42, 44, 55).

Both the helicase and C-terminal domain (CTD) of RIG-I bind to RNA, but it is the CTD that is responsible for the recognition of the 5′ triphosphate double-stranded structure typical of viral RNA (16, 39, 40). Recently, Rehwinkel et al. showed that the physiological ligand of RIG-I during influenza A virus or SeV infection is the full-length viral genomic single-stranded RNA (ssRNA), which possesses base-paired regions or defective interfering (DI) genomes (35). In contrast to RIG-I, MDA5 recognizes long viral double-stranded RNA (dsRNA) (21). The RNA binding activity of the MDA5 CTD is relatively weak compared with that of the RIG-I CTD, because the basic surface of the MDA5 CTD has a more extensive flat region than the RIG-I CTD (8, 45, 46). Although the RNA binding activity of the MDA5 CTD is weak, this protein plays a pivotal role in the recognition of picornavirus RNA (20, 21).

For the efficient recognition of viral RNA, RIG-I and MDA5 require protein modification and association with upstream factors. LGP2 is one of the upstream factors. LGP2 lacks an N-terminal CARD; thus, LGP2 itself cannot transmit the signal in the absence of RIG-I or MDA5 (36, 38, 49). The CTD of LGP2, which binds to the terminal region of viral double-stranded RNA, is more similar to the CTD of RIG-I than to that of MDA5 (24, 33, 45). LGP2 knockout studies have revealed that LGP2 is essential for type I IFN production by MDA5 but plays only a minor role in type I IFN production by RIG-I (38, 49). RIG-I requires modification of K63-linked polyubiquitination by TRIM25 and Riplet/REUL ubiquitin ligases for its full activation (11, 13, 30, 31). High-mobility-group box (HMGB) proteins also act as upstream factors of RLRs. Recently, Yanai and colleagues reported that HMGB1, HMGB2, and HMGB3 serve as sentinels for the nucleic acids required for both RIG-I and MDA5 recognition of viral RNA (56). Hayakawa and colleagues reported that ZAPS associates with RIG-I to promote oligomerization and ATPase activity of RIG-I (15). Another factor interacting with RLRs is DDX3, a DEXD/H box RNA helicase, which is similar to LGP2 in that it does not contain a CARD but promotes signaling by forming a complex with either RIG-I or MDA5 (32). DDX3 also plays important roles in TBK-1- and IKK-ε-mediated IRF activation, and Schröder et al. and Soulat et al. were the first to describe results showing that DDX3 is a non-RLR helicase involved in innate immune responses (41, 43).

DDX60, a DEXD/H box helicase, was annotated in a genome project, and the protein function is unknown. The protein is weakly similar to SKIV2L and SKIV2L2 and is the

* Corresponding author. Mailing address: Department of Microbiology and Immunology, Graduate School of Medicine, Hokkaido University, Kita-15, Nishi-7, Kita-ku, Sapporo 060-8638, Japan. Phone: 81-11-706-5056. Fax: 81-11-706-7866. E-mail: oshiumi@med.hokudai.ac.jp.

† Supplemental material for this article may be found at http://mcb.asm.org/.

▽ Published ahead of print on 2 May 2011.

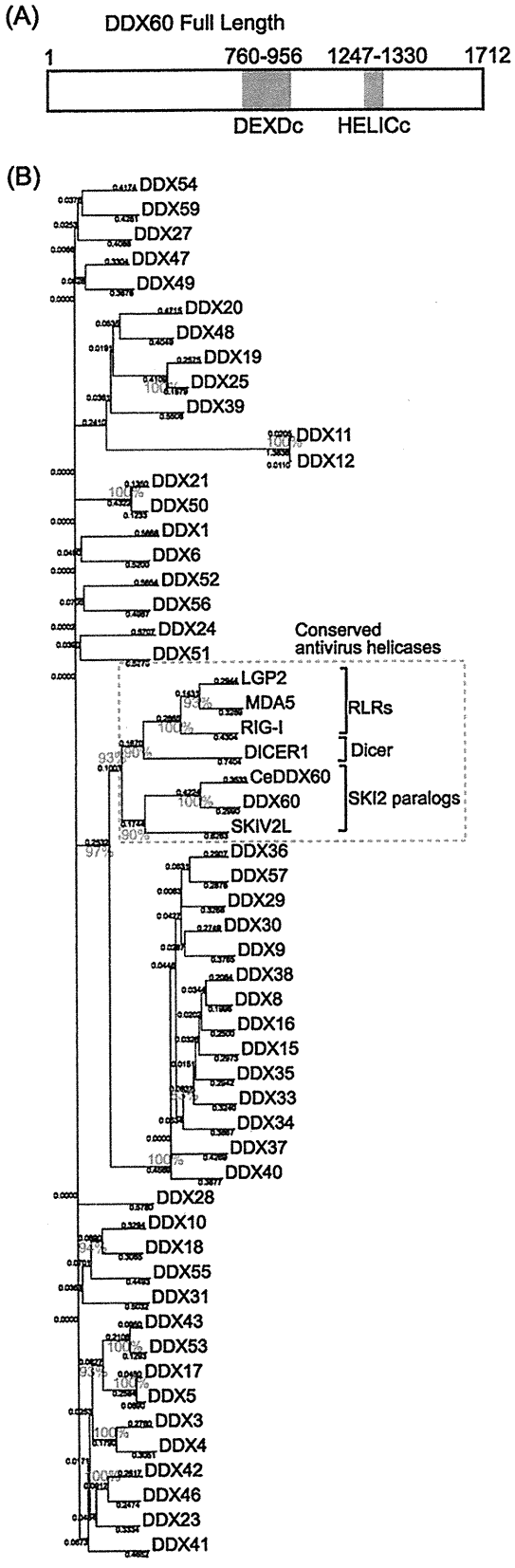

FIG. 1. The phylogenetic tree of DEXD/H box RNA helicase. (A) Schematic diagram of DDX60. DDX60 encodes a peptide of 1,712 amino acids (aa) that contains a DEXD/H box (DEXDc; aa 760 to 956) and HELICc (aa 1247 to 1330). (B) The phylogenetic tree of DEXD/H box RNA heliases. Ce, *C. elegans*. The bootstrap probabilities and genetic distances are shown in red and black, respectively.

human homolog of *Saccharomyces cerevisiae* (budding yeast) Ski2, a cofactor of the RNA exosome (9, 18). The RNA exosome is a macromolecular protein complex that includes ribonucleases and helicases and controls the quality of host RNA molecules in both the nucleus and cytoplasm (17). It is composed of nine core components and several cofactor proteins (18). In budding yeast, the RNA exosome and Ski2 together exhibit antiviral activity (53, 54); similarly, the mammalian RNA exosome, together with its cofactors, shows antiviral activity against Moloney leukemia virus and Sindbis virus (5, 14). Our microarray analysis has shown that DDX60 is upregulated in human dendritic cells during infection with measles virus (MV) (our unpublished results). Thus, we expected DDX60 to be a novel antiviral protein and found that DDX60 is involved in RIG-I-like receptor-dependent antiviral pathways.

Here, we show that DDX60 is induced during viral infection and suppresses viral replication. DDX60 was found to form a complex with RLRs, promoting signaling; the results of knockdown experiments indicated that DDX60 is involved in RLR-dependent pathways. Moreover, the DDX60 helicase domain was observed to bind to viral RNA and DNA. Furthermore, DDX60 is required for type I IFN expression after DNA virus infection. These data indicate that DDX60 is a novel antiviral helicase involved in RLR-dependent pathways.

MATERIALS AND METHODS

Cell cultures. HEK293 and Vero cells were cultured in Dulbecco's modified Eagle's medium with 10% heat-inactivated fetal calf serum (Invitrogen), and HeLa cells were cultured in minimum Eagle's medium with 2 mM L-glutamine and 10% heat-inactivated fetal calf serum (JRH Biosciences). HEK293FT cells were maintained in Dulbecco's modified Eagle's high-glucose medium containing 10% heat-inactivated fetal calf serum (Invitrogen). RAW 264.7 cells were cultured in RPMI 1640 medium with 10% heat-inactivated fetal calf serum (Invitrogen). Mouse bone marrow-derived dendritic cells (BM-DCs) were induced as described in reference 2. PV receptor (PVR)-transgenic mice were provided by S. Koike (Tokyo Metropolitan Institute for Neuroscience).

Plasmids. Full-length human DDX60 cDNA was obtained from HeLa cell total RNA by reverse transcription-PCR (RT-PCR). The obtained cDNA fragments were sequenced, and we confirmed by PCR that the obtained cDNA clones do not contain nucleotide mutations. The DDX60 cDNA clone was cloned into XhoI and NotI restriction sites of pEF-BOS, and a hemagglutinin (HA) tag sequence was inserted just before the stop codon. EXOSC1, EXOSC4, or EXOSC5 was amplified by RT-PCR from HeLa cell total RNA. The obtained cDNA fragment was cloned into XhoI and NotI restriction sites of pEF-BOS vector, and the FLAG tag was fused at the C-terminal end. The DDX6 cDNA carrying a full-length open reading frame (ORF) was amplified by RT-PCR using primers DDX6-F (GGC CGC TCG AGC CAC CAT GAG CAC GGC CAG AAC AGA G) and DDX6-R (GGC GGG GTA CCC CAG GTT TCT CAT CTT CTA CAG). The fragment was cloned into XhoI and NotI sites of pEF-BOS vector. For *in vitro* viral RNA synthesis, we amplified VSV-G region cDNA by PCR using primers VSV-G-F and VSV-G-R. The obtained cDNA fragment was cloned into pGEM-T Easy vector. The primer sequences are as follows: for VSV-G-F, ACAGGAGAATGGGTTGATTC; and for VSV-G-R, ATGCAAA GATGGATACCAAC. Vectors expressing full RIG-I or RIG-I fragments were described before (30). The plasmids expressing TLR3 or TICAM-1 are described in reference 29. The p125luc reporter plasmid was a gift from T. Taniguchi (University of Tokyo, Tokyo, Japan). Mutant DDX60 expression constructs were

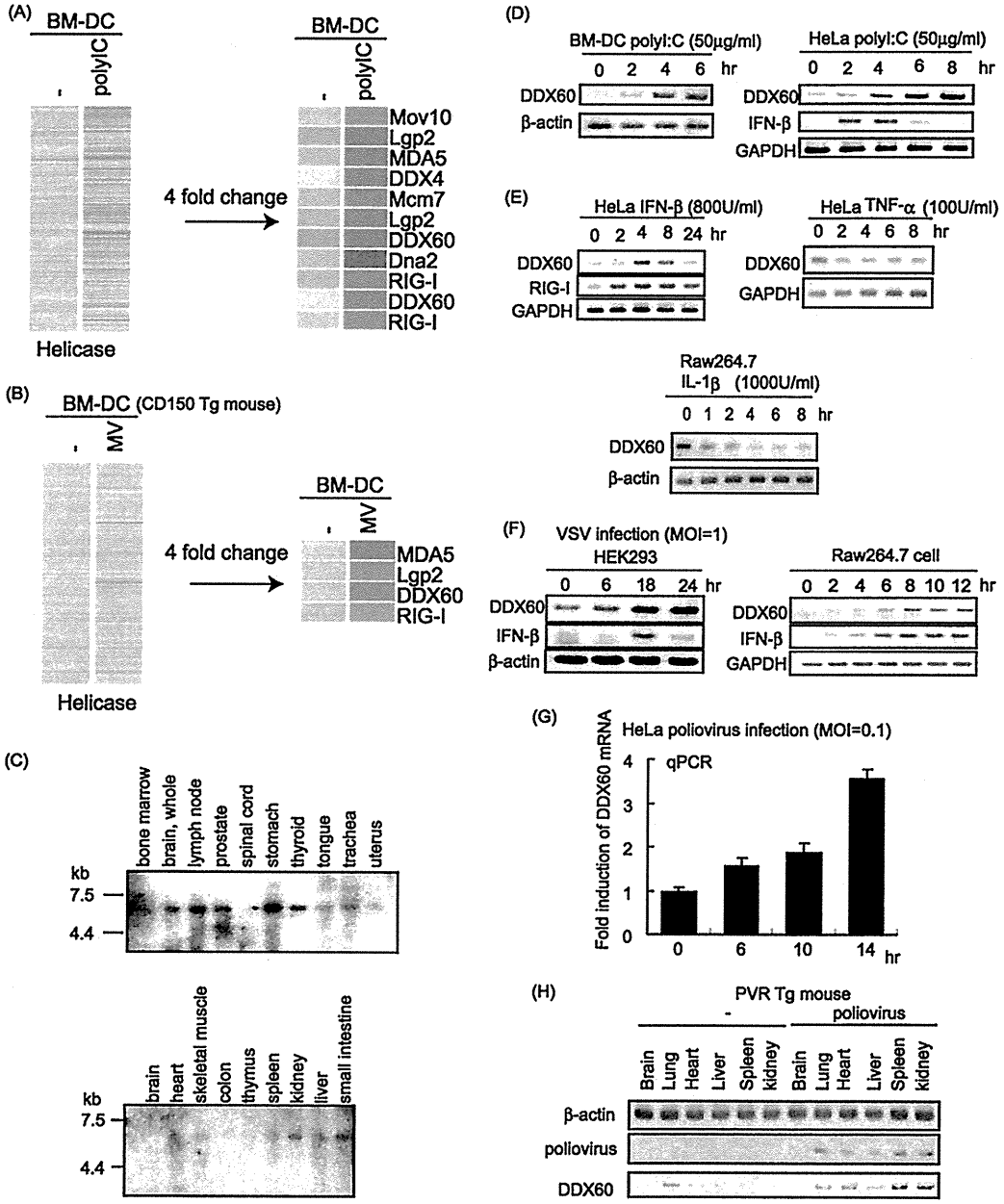

FIG. 2. Expression of DDX60 mRNA. (A and B) Mouse BM-DCs were stimulated with poly(I · C) (A) or infected with MV in the presence of anti-IFN-AR antibody (B). Total RNA was extracted from the cells, and microarray analysis was performed. The heat maps in the left column show the expression profiles of the genes encoding the helicase domain. The heat maps in the right column show the genes encoding the helicase domain whose expression levels changed more than 4-fold. (C) Northern blot of human DDX60 mRNAs in specified tissues. Northern blots of human tissues were probed with DDX60 cDNA. (D and E) Mouse BM-DCs, HeLa cells, or RAW 264.7 cells were stimulated with 50 μg of poly(I · C)/ml (D), 800 U of IFN-β/ml (E), 100 U of TNF-α/ml (E), or 1,000 U of IL-1β/ml (E). Expression of DDX60, RIG-I, GAPDH (glyceraldehyde-3-phosphate dehydrogenase), and β-actin mRNA was examined by RT-PCR. (F and G) HEK293 cells, RAW 264.7 cells, or HeLa cells were infected with VSV at an MOI of 1 (F) or PV at an MOI of 0.1 (G). Expression of DDX60, IFN-β, β-actin, and/or GAPDH was examined by RT-PCR (F) or RT-qPCR (G). (H) PV was injected intraperitoneally (i.p.) into PVR-transgenic mice susceptible to PV. Tissue RNA extraction was performed before or 3 days after infection, and RT-PCR was carried out on these samples.

amplified using primers for DDX60 (amino acids [aa] 1 to 169), (aa 169 to 334), (aa 334 to 490), (aa 478 to 656), (aa 657 to 857), (aa 857 to 1054), (aa 1049 to 1256), (aa 1256 to 1409), (aa 1407 to 1543), and (aa 1543 to 1712). The primer sequences are shown in Table S1 in the supplemental material.

Phylogenetic analysis. The amino acid sequences of the DEXD/H box domain were aligned using ClustalW software on the NIG server. The phylogenetic tree was drawn using the neighbor-joining method and GENETYX-MAC software (version 13.0.3).

Northern blotting. A human DDX60 644-bp cDNA fragment (from the region at bp 3978 to 4621) was used for the probe for Northern blotting. The Northern blot membranes (human 12-lane multiple-tissue Northern [MTN] blot and MTN blot III) were purchased from Clontech. The probe was labeled using